CHAPTER 5

RESULTS AND DISCUSSION

In this chapter, the results on current-voltage characteristic measurement of SLG/Mo/Cu(In,Ga)Se_2/CdS/ZnO structure are discussed. Firstly, I will describe the model used to analyze the standard J-V characteristics measurement at room temperature. Secondly, the influence of impurity concentration and light intensity on the CIGS-based thin film solar cell performance and J-V characteristics are shown. The analysis of the temperature dependence J-V characteristics is shown in the third part. The last part of this chapter, I will propose the possible current mechanism and the band alignment of SLG/Mo/Cu(In,Ga)Se_2/CdS/ZnO heterojunction thin film used in this experiment.

5.1 Results and the Analysis of J-V Characteristics

ศูนย์วิทยทรัพยากร
จุฬาลงกรณ์มหาวิทยาลัย

The CIGS-based thin film solar cells with different elemental composition were characterized by the current-voltage (J-V) response, measured at 25 °C under 100 mW/cm^2 (AM1.5 illumination). The analysis of the J-V curves was carried out to characterize the diode behavior.

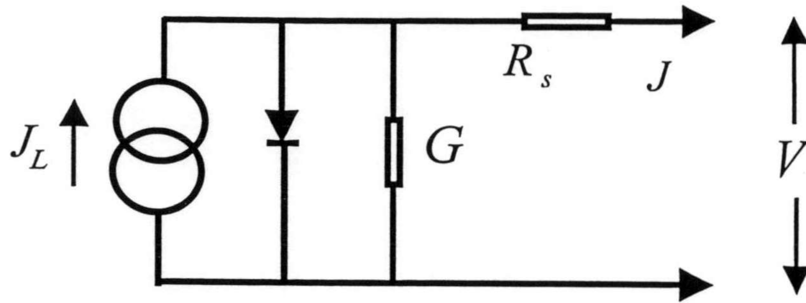

Figure 5.1: The equivalent circuit of a solar cell.

The J-V characteristics in light and dark were compared to verify whether the light characteristic was essentially a translated curve with light short circuit current, J_{sc} or J_L (see Fig. 5.2). The characterization of J-V characteristic of sample no.176-R8C3 which use one diode model (see detail in chapter 4) were shown in Figs. 5.2-5.5.

$$J = J_0\left[\exp\left(\frac{q(V - R_s J)}{AkT}\right) - 1\right] - J_L + GV \tag{5.1}$$

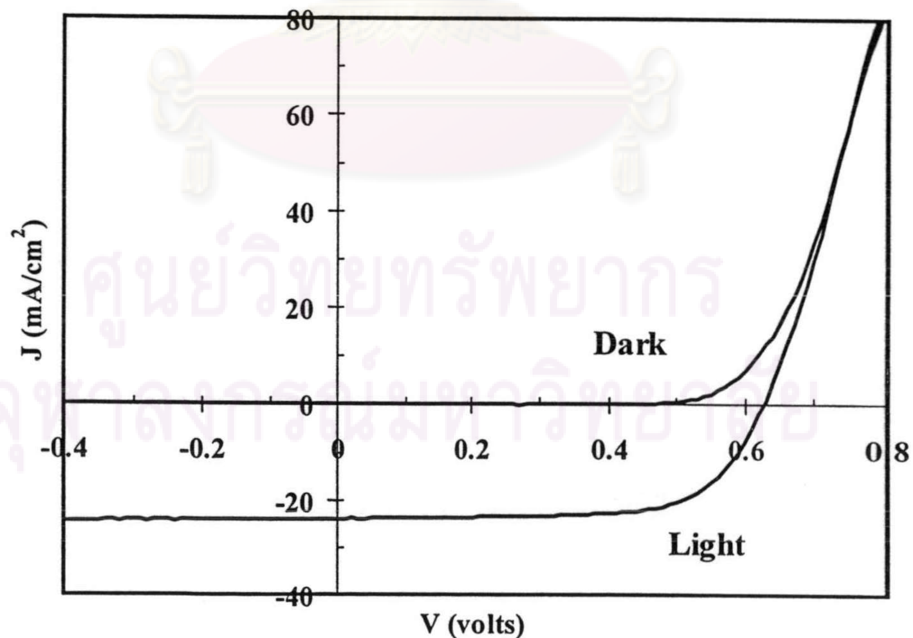

Figure 5.2: Example of the J-V curve of CIGS-based solar cell no.176-R8C3 at standard measurement (under dark and AM1.5 illumination)

The shunt conductance G, was obtained from the minimum value of the slope dJ/dV in reverse bias (see Fig. 5.3) and used to calculated $J' = J - GV$.

The dJ/dV versus V curve yields shunt conductance (see Fig. 5.3). For all devices, the dark shunt term was small enough, so that it can be neglected in the subsequent analysis. The light curve showed a slight change of current collection with voltage. The un-smoothed light curve was noisy due to flicker in ELH type halogen lamp powered by AC source. The scatter was reduced by using the value of dJ/dV calculated by the three-point average.

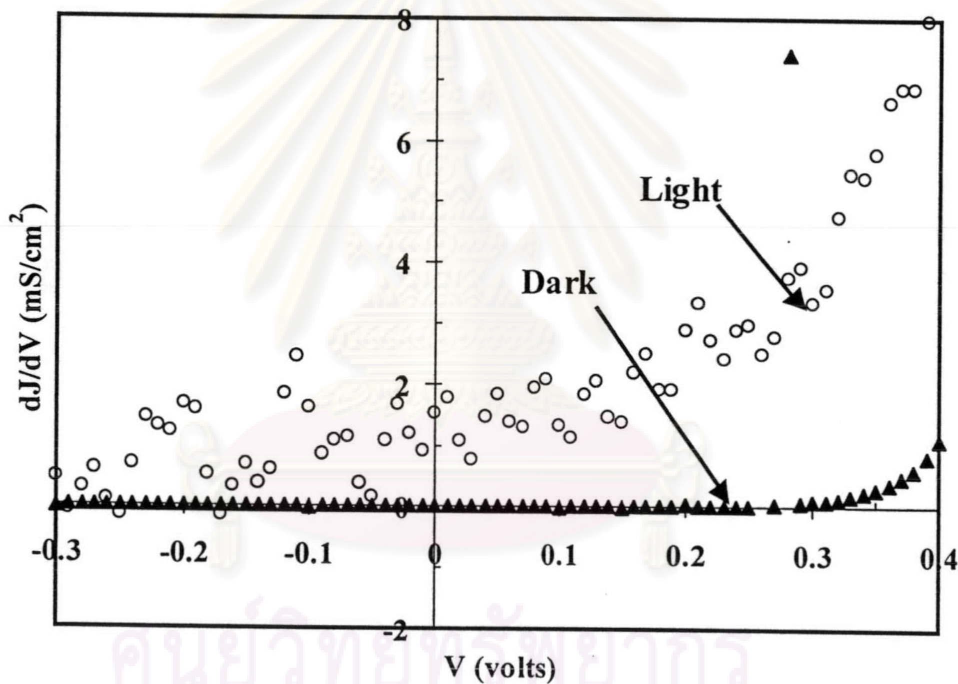

Figure 5.3: Illumination and dark dJ/dV for the sample no.176-R8C3.

With $R_s G << 1$, differentiating Eq. (5.1) gives

$$\frac{dV}{dJ'} = R_s + \frac{AkT}{q}(J' + J_{sc})^{-1} \tag{5.2}$$

The series resistance, R_s, was obtained from the intercept and slope of a linear fit to dV/dJ' plotted versus $(J' + J_{sc})^{-1}$ (see Fig. 5.4).

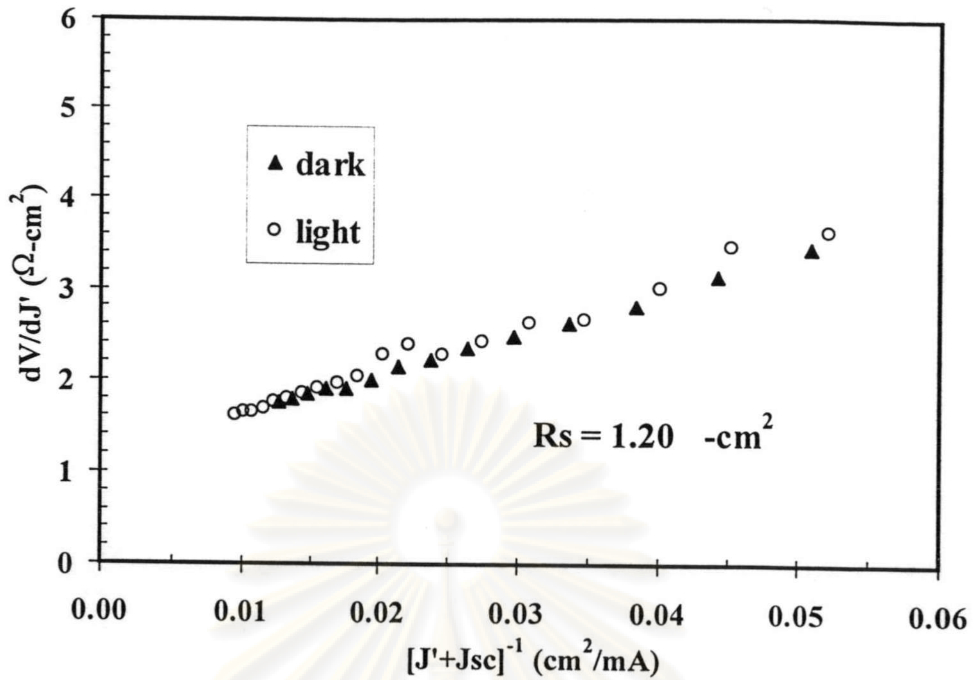

Figure 5.4: Illumination and dark dV/dJ' vs $(J'+J_{sc})^{-1}$ for sample no. 176-R8C3. Straight lines show the fit to determine R_s.

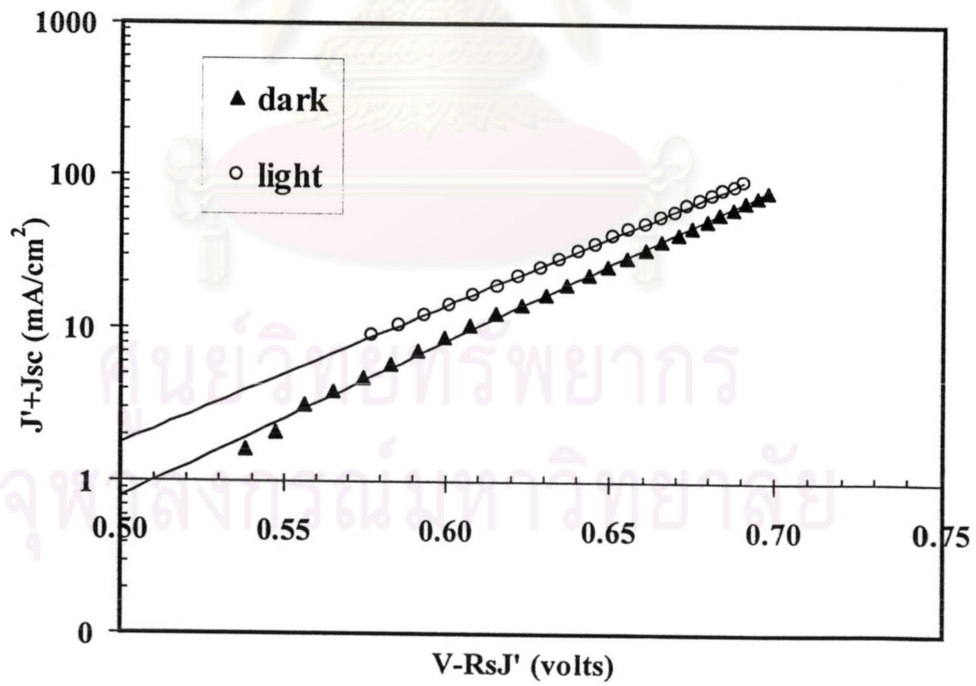

Figure 5.5: Logarithmic plot of $J'+J_{sc}$ vs $V-R_sJ'$ both in dark and illumination for sample no. 176-R8C3. Straight lines show the fit to determine J_0 and A.

By using the value of R_s, the forward current J_0 and diode ideality factor A were obtained from the intercept and slope of linear fit in the logarithmic plot of $J'+J_{sc}$ versus $V-R_sJ'$ (see Fig. 5.5). The results of the diode analysis for the J-V data from 15 samples under standard J-V measurement are summarized in Table 5.1.

Table 5.1 $Cu(In,Ga)Se_2$-based solar cell parameters under AM1.5 illumination at 25 °C .

Sample no.	**V_{oc} (V)**	**J_{sc} (mA/cm²)**	**FF (%)**	**η (%)**	**G (mS/cm²)**	**Rs (Ω-cm²)**	**Dark**		**Illuminated**	
							J_0 (mA/cm²)	**A**	**J_0 (mA/cm²)**	**A**
176-R8C1	0.60	22.96	65.39	9.01	0.019	0.703	4.0×10^{-6}	1.56	9.0×10^{-5}	1.86
176-R5C1	0.61	25.92	70.20	11.10	0.005	0.703	4.0×10^{-6}	1.53	4.0×10^{-5}	1.73
176-R6C5	0.62	23.69	66.65	9.79	0.032	1.340	4.0×10^{-5}	1.86	8.0×10^{-5}	1.90
176-R1C3	0.63	26.20	64.33	10.62	0.026	1.288	6.0×10^{-6}	1.64	7.0×10^{-5}	1.88
176-R8C3	0.63	24.01	67.74	10.25	0.003	1.174	7.0×10^{-6}	1.66	6.0×10^{-5}	1.86
171-R8C1	0.50	22.71	69.23	7.86	0.016	0.785	9.0×10^{-5}	1.58	2.0×10^{-4}	1.67
171-R4C1	0.53	29.85	70.17	11.10	0.033	0.836	5.0×10^{-5}	1.54	6.0×10^{-5}	1.55
171-R6C3	0.54	27.49	67.89	10.08	0.011	1.269	6.0×10^{-5}	1.63	1.0×10^{-4}	1.66
171-R2C1	0.54	28.13	68.17	10.35	0.252	0.877	1.0×10^{-5}	1.45	5.0×10^{-5}	1.57
171-R4C2	0.54	30.84	67.99	11.32	0.036	1.329	4.0×10^{-5}	1.59	5.0×10^{-5}	1.57
164-R4C2	0.47	33.11	63.62	9.90	0.019	1.105	7.0×10^{-4}	1.72	1.6×10^{-3}	1.82
164-R5C4	0.47	28.93	63.35	8.61	0.185	1.383	9.0×10^{-4}	1.77	1.6×10^{-3}	1.84
164-R2C3	0.49	29.16	65.67	9.38	0.417	1.232	3.0×10^{-4}	1.68	1.3×10^{-3}	1.88
164-R4C5	0.49	27.59	63.52	8.59	0.824	1.400	5.0×10^{-4}	1.75	9.0×10^{-4}	1.80
164-R6C1	0.49	30.54	64.89	9.71	0.002	1.002	3.0×10^{-4}	1.70	1.2×10^{-3}	1.85

Analysis of the J-V show that the $Cu(In,Ga)Se_2$ based thin film solar cells are good behavior, i.e. the J-V results can be described by the standard diode equation (Eq. (5.1)). From Table 5.1, all values of diode ideality factor are between 1 and 2,

correspond with the mechanism controlling the junction behavior in these solar cells; Shockley-Read-Hall (SRH) recombination in the space charge region of the $Cu(In,Ga)Se_2$.

From the above results, most samples in Table 5.1 show very high R_s compared with CIGS-based solar cell with efficiency ~ 10% (R_s < 0.1Ω-cm² [20]). With the high R_s and the current collection dependent of voltage (J_L is not constant), the superposition principle no longer holds and the light J-V curve cannot be described by a simple translation of the dark curve. Therefore, the determination of diode parameters with high R_s devices by using Eqs. 4.6 – 4.8 gives high error since the assumption that the J_L is constant, and $R_s G << 1$ is not valid. The main effect of the high R_s or low R_{sh} is decrease the fill factor and the solar cell performance, so that it is important to lower the R_s of our CIGS-based solar cell samples to obtain the higher cell performance.

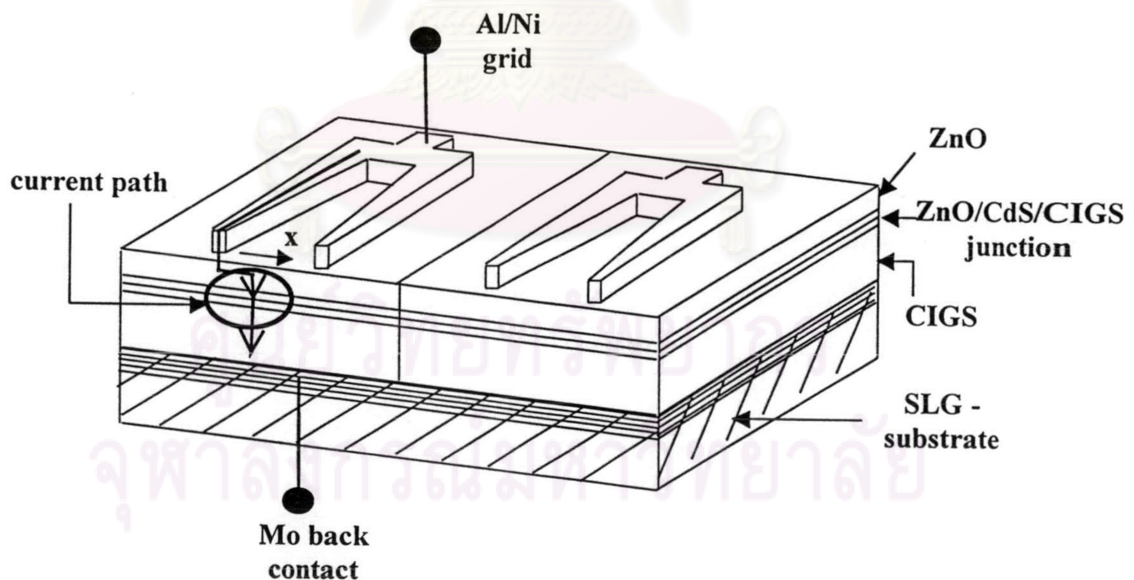

Figure 5.6: Possible distributed resistance model.

Figure 5.6 shows the possible causes of series resistance in our CIGS-based thin film solar cell which have following contributions:

- Resistance of the front grid structure,
- Contact resistance,
- Resistance of the back contact sheet,
- The lateral resistance to current flow along the plane of the film depending on the distance x.
- The transverse resistance through the base layer.

However, there are some $Cu(In,Ga)Se_2$-based thin film solar cells which cannot be represented in terms of simple superposition of photocurrent and forward diode current in the dark. The J-V characteristics of these samples were shown in the next section.

5.2 The Impurity Concentration in CBD-CdS Effects

The purpose of this experiment in this section is to investigate the influence of the bulk properties of the CBD-CdS buffer layer on the performance of the $Cu(In,Ga)Se_2$–based thin film solar cells. All three samples investigated in this experiment had the SLG/Mo/$Cu(In,Ga)Se_2$/CBD-CdS/ZnO/Ni(Al) structure prepared with the same process as described in the previous chapter. The different between three samples is the thiourea concentration in the CdS buffer layer. The standard solutions in the CBD-CdS process contain 0.004M $CdSO_4$ and 4.0M NH_3 but thiourea concentration was varied between 0.03M and 0.1M while the thickness of CBD-CdS layer was kept constant. After completion of the device, the whole piece was scribed into 40 cells as shown in Fig. 5.7. Table 5.2 summarizes the preparation conditions for the CBD-CdS buffer layer.

Table 5.2: Preparation conditions for the CBD-CdS buffer layer.

Sample no.	**Thiourea conc. (M)**	**Chemical Bath Temperature (°C)**	**Deposition Time (minutes)**
156	0.03	60	6
157	0.06	60	8
158	0.1	60	10

1	**9**	**17**	**25**	**33**
2	**10**	**18**	**26**	**34**
3	**11**	**19**	**27**	**35**
4	**12**	**20**	**28**	**36**
5	**13**	**21**	**29**	**37**
6	**14**	**22**	**30**	**38**
7	**15**	**23**	**31**	**39**
8	**16**	**24**	**32**	**40**

Figure 5.7: Schematic of 40 individual CIGS-based thin film solar cells on each sample no. The numbers on the schematic represent the position of each cell.

The standard I-V results of the $Cu(In,Ga)Se_2$ – based thin film solar cells no.156, 157, and 158 were shown in Figs. 5.8 – 5.10. These show the crossover effect or the distortion in the illuminated I-V curves. In other words, the superposition principle of the illuminated and dark I-V curve is no longer valid. Each position on the same sample has very different degree of crossover. Some positions show the good I-V and some positions show very high degree of crossover. From these results, the appearance of crossover effect in the I-V characteristics is independent of the thiourea concentration. This indicates that it is quite difficult to determine the optimized condition of thiourea concentration in our CBD-CdS process. The main cause is due to the uniformity of elemental composition in the $Cu(In,Ga)Se_2$ absorber layer. It has been seen that more [Cu]/([Ga]+[In]) ratio, more quickly the colloid formed within the CBD solution and they have variety of possible products of the CBD reaction that is the effect of the

exchange reactions occurring at the interface of the CIGS and CdS. It means that a small variation in the CBD process chemistry may have a significant influence on the CdS/CIGS interface and on the performance of the resulting devices.

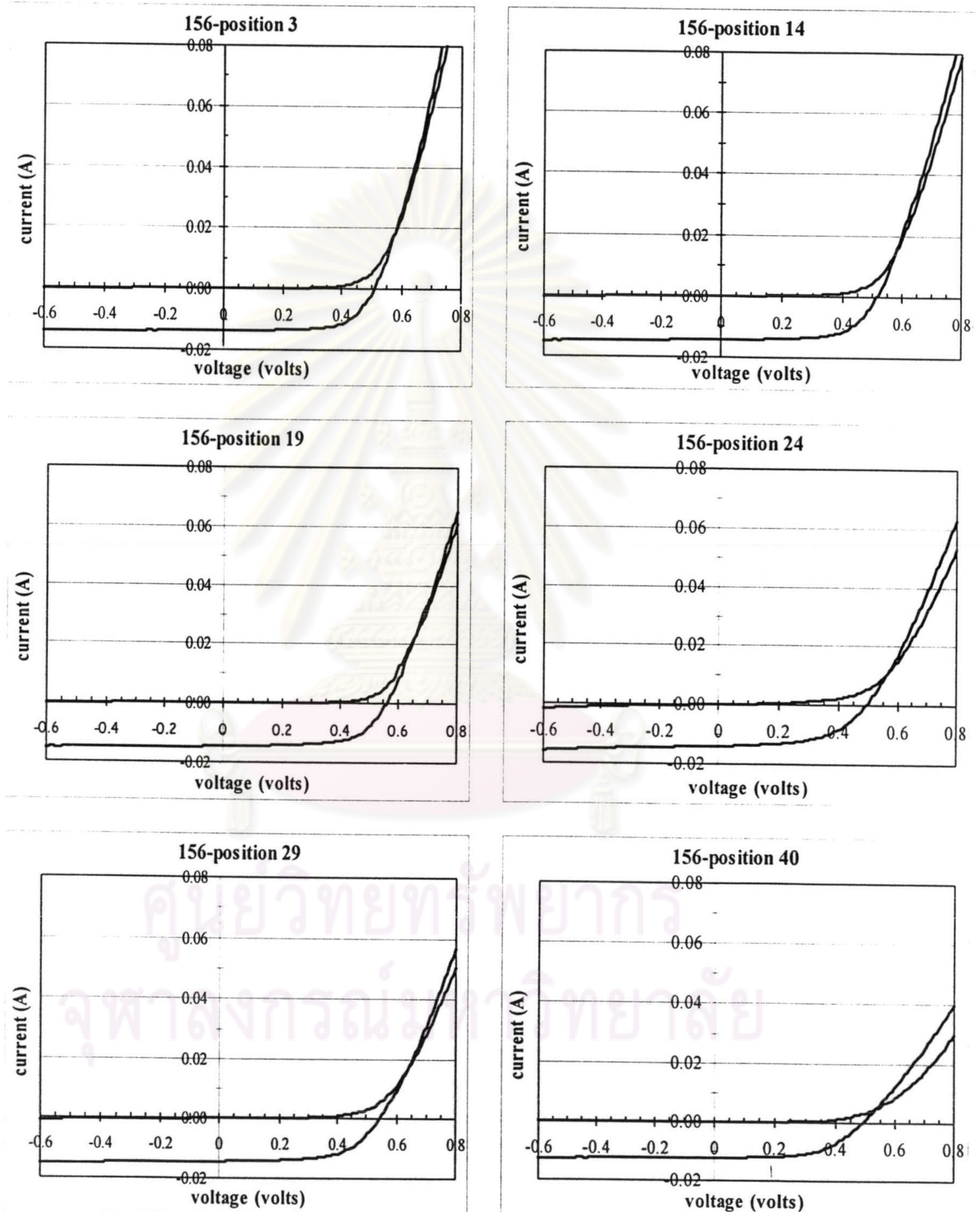

Figure 5.8: The dark and illumination I-V characteristics of sample no. 156 (Thiourea conc. 0.03M) at different position.

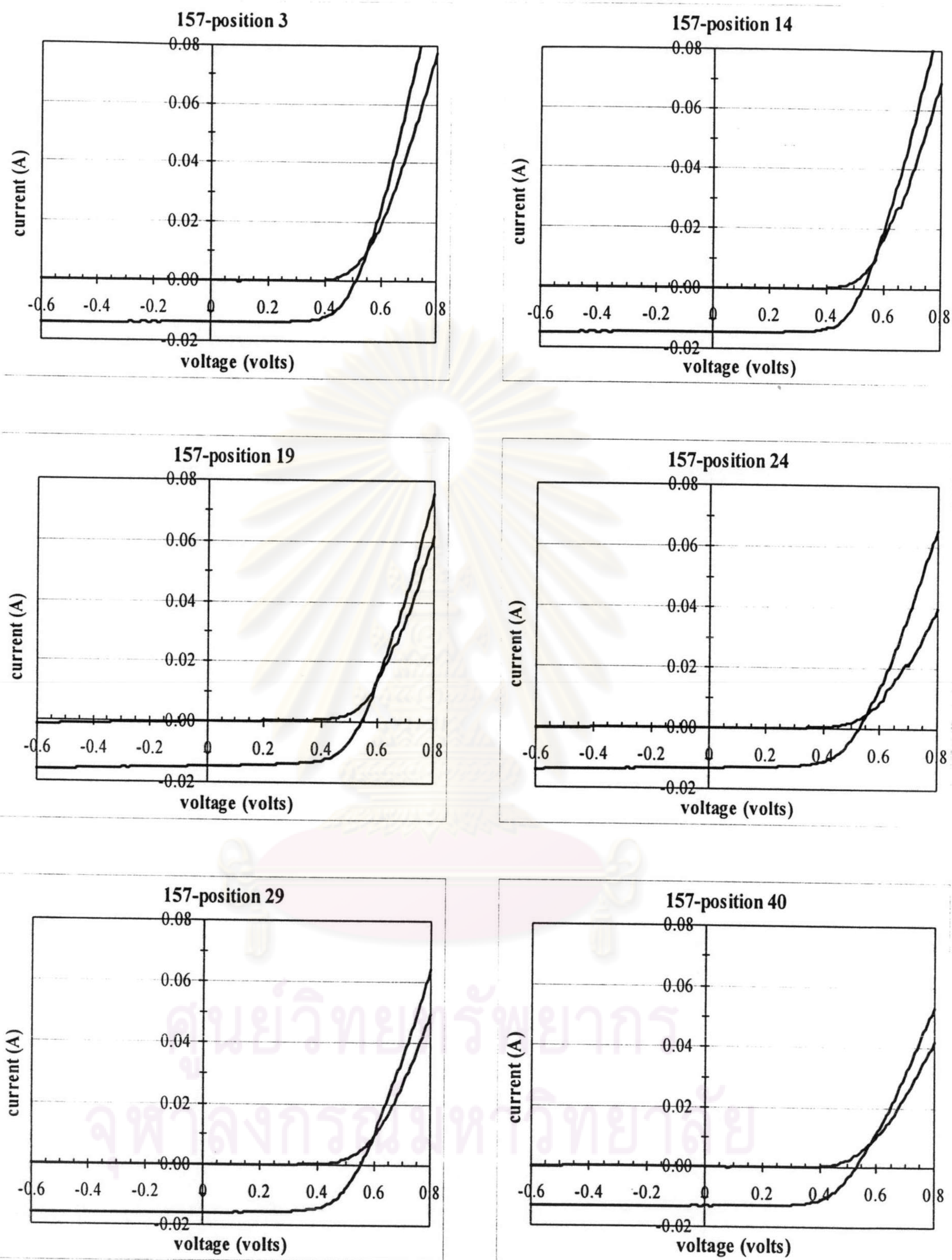

Figure 5.9: The dark and illumination I-V characteristics of sample no. 157 (Thiourea conc. 0.06M) at different position.

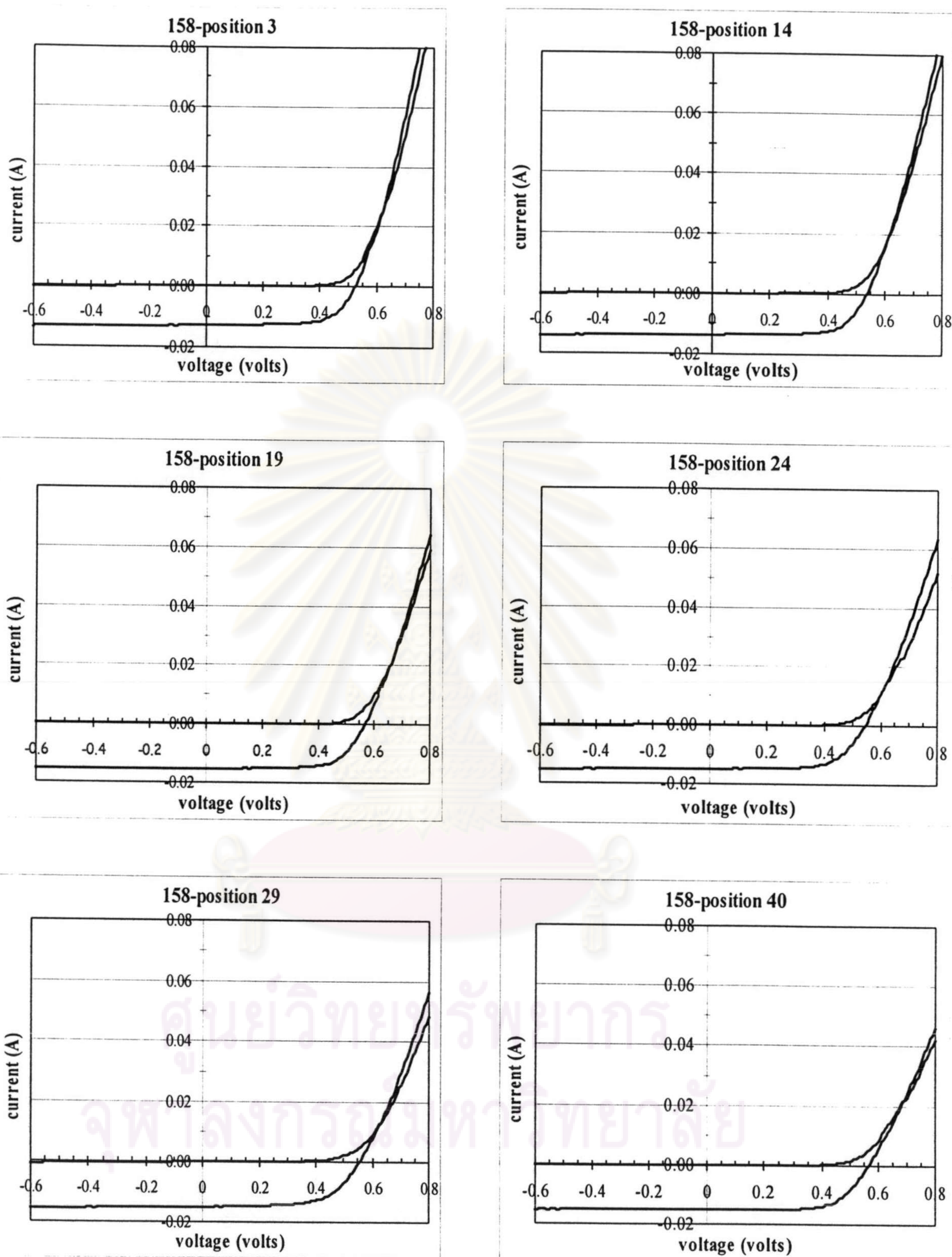

Figure 5.10: The dark and illumination I-V characteristics of sample no. 158 (Thiourea conc. 0.1M) at different position.

ศูนย์วิทยทรัพยากร
จุฬาลงกรณ์มหาวิทยาลัย

In order to find the optimal impurity concentration in the CBD-CdS layer in our experiment, the average solar cell parameters of all 40 individual cells of each sample were considered.

The CIGS-based thin film solar cell parameters (J_{sc},V_{oc},FF,η) with three different thiourea concentration were presented in Fig. 5.11 – 5.14.

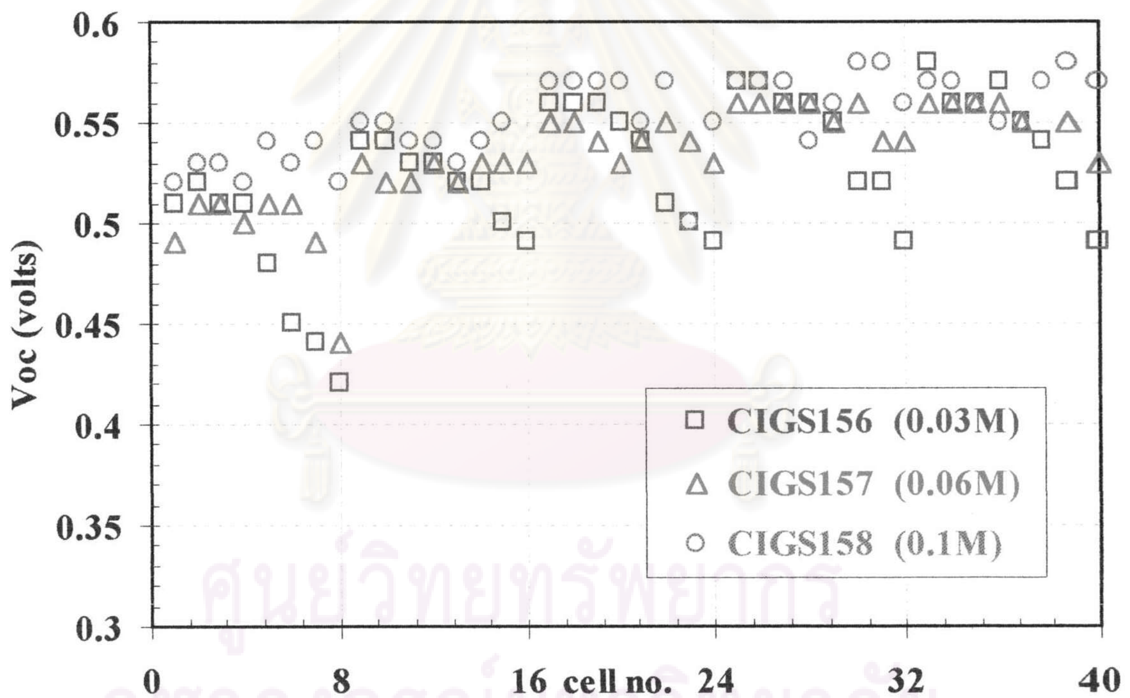

Figure 5.11: Variation in the open-circuit voltage V_{oc} of 40 individual CIGS-based thin film solar cells in this experiment.

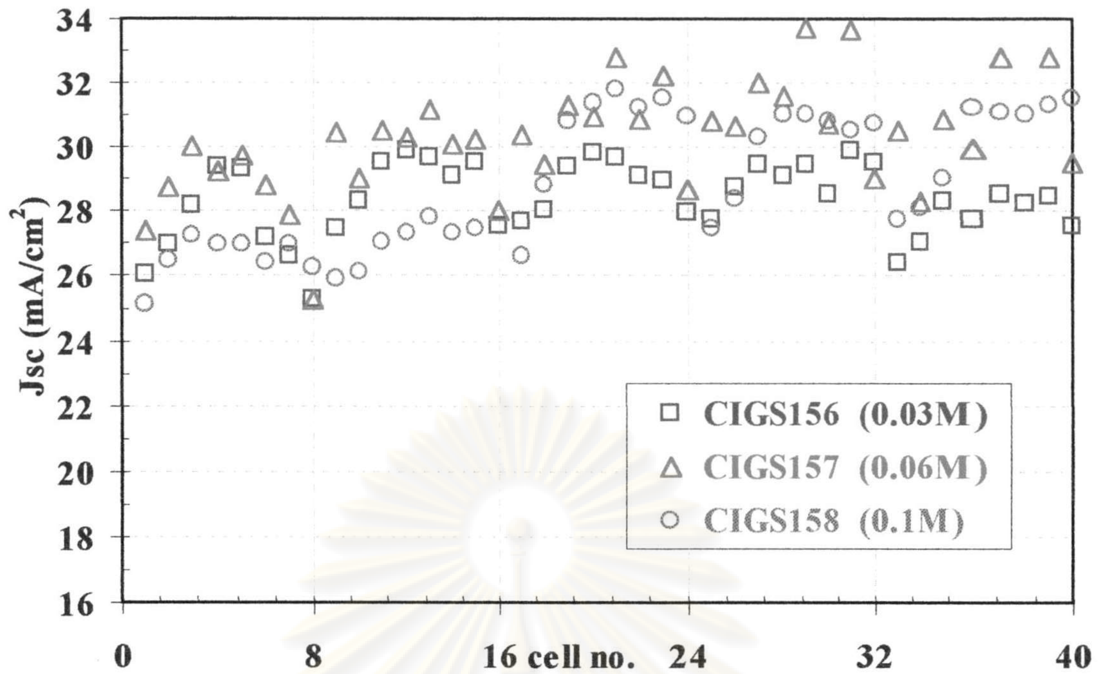

Figure 5.12: Variation in the short circuit current density J_{sc} of 40 individual CIGS-based thin film solar cells in this experiment.

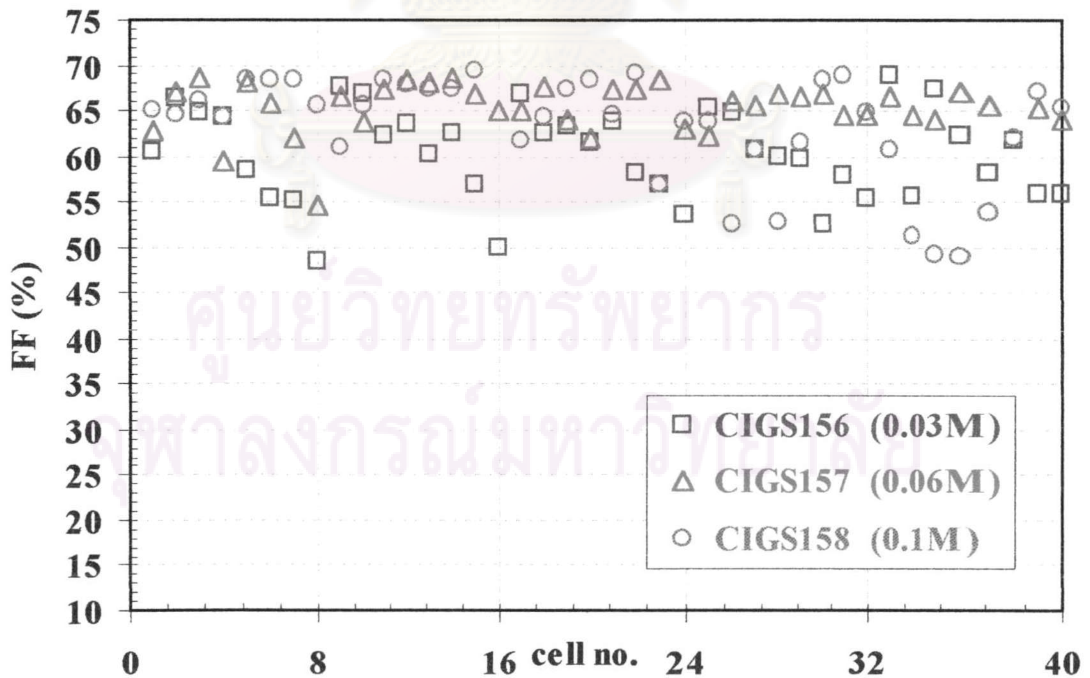

Figure 5.13: Variation in the fill factor *FF* of 40 individual CIGS-based thin film solar cells in this experiment.

ศูนย์วิทยทรัพยากร
จุฬาลงกรณ์มหาวิทยาลัย

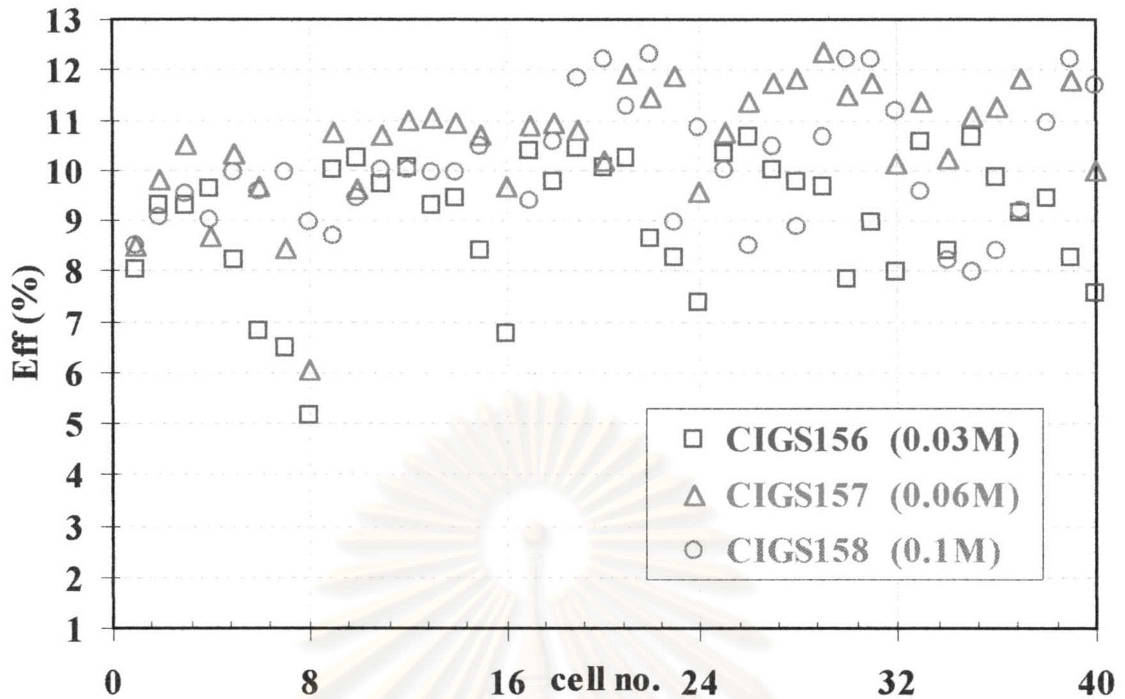

Figure 5.14: Variation in the efficiency η of 40 individual CIGS-based thin film solar cells in this experiment.

Table 5.3: Statistics of all the solar cell parameters for each sample made into cells as a function of thiourea concentration. Sample no.156 (0.03M), no.157 (0.06M), no.158(0.1M).

Sample no.	Total # of cells	V_{oc} (volts)				J_{sc} (mA/cm^2)				FF (%)				η (%)			
		Max	Min	Mean	S.D	Max	Min	Mean	S.D	Max	Min	Mean	S.D	Max	Min	Mean	S.D
156	39	0.58	0.44	0.52	0.03	29.8	26.0	28.4	1.05	68.8	49.9	60.5	4.64	10.6	6.45	9.11	1.16
157	39	0.56	0.44	0.53	0.02	33.7	25.2	30.3	1.75	68.6	54.5	65.3	2.80	12.3	6.05	10.6	1.22
158	39	0.58	0.50	0.55	0.02	31.7	25.1	28.8	2.10	69.4	48.8	63.2	5.89	12.2	7.97	10.0	1.26

ศูนย์วิทยทรัพยากร จุฬาลงกรณ์มหาวิทยาลัย

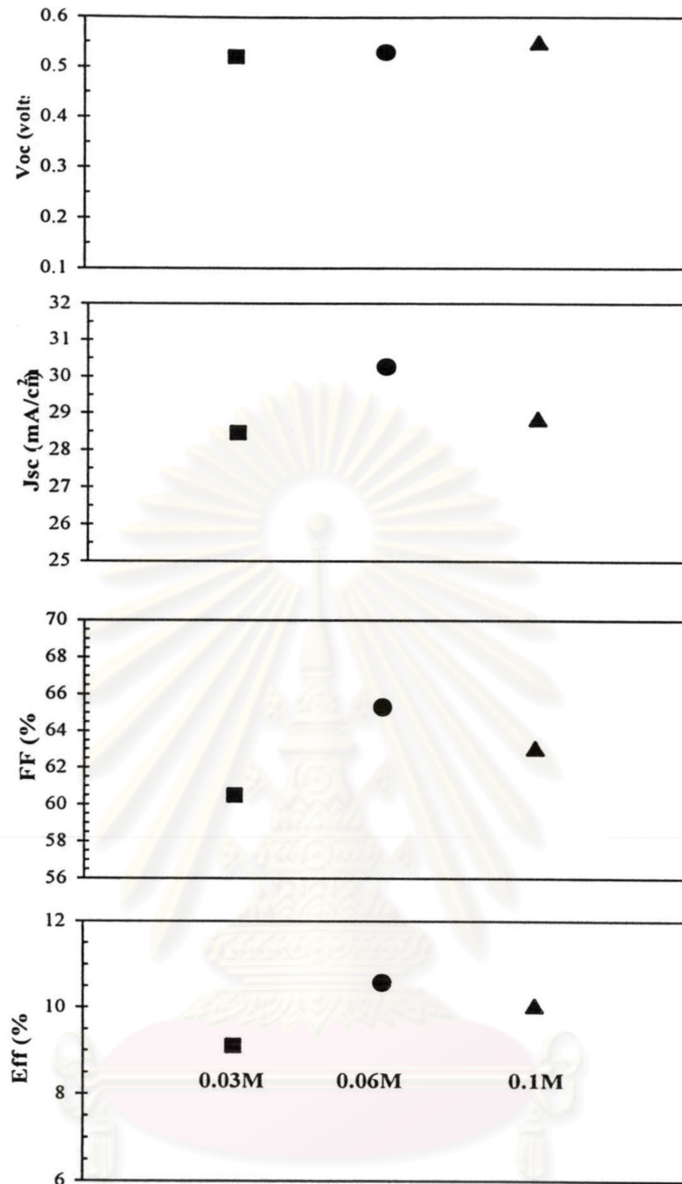

Figure 5.15: Variation in solar cell parameters with thiourea concentration for CBD-CdS buffer layer.

Table 5.3 and Fig. 5.15 show the average CIGS-based solar cell parameters along with their standard deviation. In spite of the samples were not processed at the same time in the Cu(In,Ga)Se_2 evaporation runs or under the same time in the ZnO window layer fabrication after the CBD-CdS process, they still give an idea of the sample to sample variation, and the cell to cell variation within each sample. From

these results, the thiourea concentration of 0.06M gives us the highest average solar cell parameters as long as we have a good quality $Cu(In,Ga)Se_2$ absorber layer.

The above results indicate that the impurity concentration in the CdS layer play the minor role in the junction formation of our CIGS-based solar cells fabricated here at the Semiconductor Physics Research Laboratory, Chulalongkorn University, which the elemental composition of $Cu(In,Ga)Se_2$ is not uniform over all the area of 5x6 cm^2. Besides this experiment, the distortion of I-V curves or the crossover effects have been frequently observed. The high-efficiency CIGS-based thin film solar cells almost always exhibit a near superposition of the I-V curve, i.e., a slight crossover at room temperature. The impurity concentration effect on the I-V characteristics performed by Kylner et al.,[17] have indicated that when the impurities or defects in the CBD-CdS layer are high enough either by increased concentration or thickness, the crossover effect appears at room temperature. However, some of these distortion I-V curves have been found to be dependent on temperature, illumination intensity that will be discussed in the next section of this chapter.

5.3 Illumination Intensity Effects

The dependence of the $Cu(In,Ga)Se_2$ – based thin film solar cell device characteristics on illumination intensity and temperature were mainly studied for the recombination mechanism at the interface or the space charge region of the heterojunction which are the key components to obtain the energy band model. In this section, the dependencies of the CIGS-based solar cell performances on illumination intensity were presented. To investigate the effect of illumination intensity, I used five CIGS-based solar cells samples with various J-V characteristics (under 100 mW/cm^2). These samples were measured at four different

illumination intensities: (1) I_o (= 100 mW/cm^2), (2) ~ 2 I_o, (3) ~ 0.58 I_o, (4) ~ 0.36 I_o. The reduction in illumination intensities were achieved by varied the distance between the ELH lamp and the sample stage. The J-V characteristics of five samples are shown in Figs. 5.16(a)-(e).

The primary change observed in Fig 5.16(c), (d), (e) is the decrease in series resistance when increase the illumination intensity (high degree of crossover) but this effect cannot be observed in Fig 5.16(a) and (b). It can be expected that the degree of change in series resistance in Fig 5.16 varies considerably with elemental composition in Cu(In,Ga)Se_2 fabrication details.

Shunt resistance is measured by the reciprocal of the slope of the J-V curves in reverse bias. The value of shunt resistance in Fig 5.16(e) changes very dramatically with illumination intensity, but slightly in Fig. 5.16(a), (c), and (d).

ศูนย์วิทยทรัพยากร

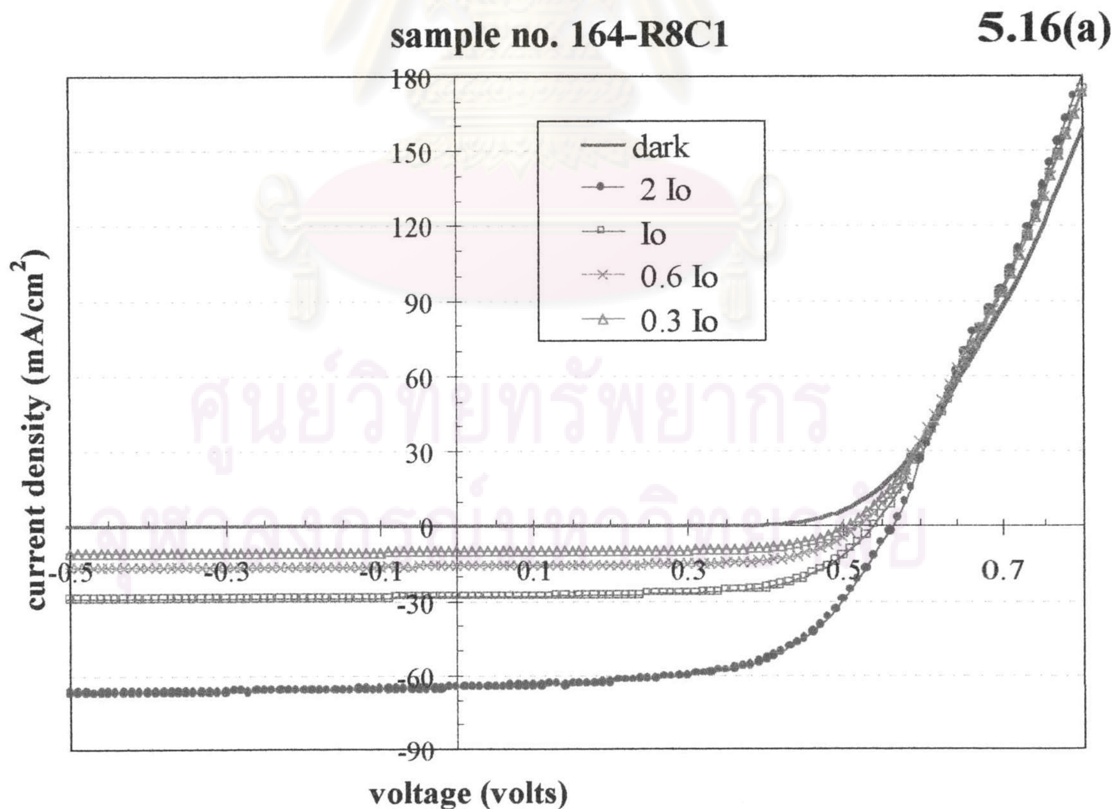

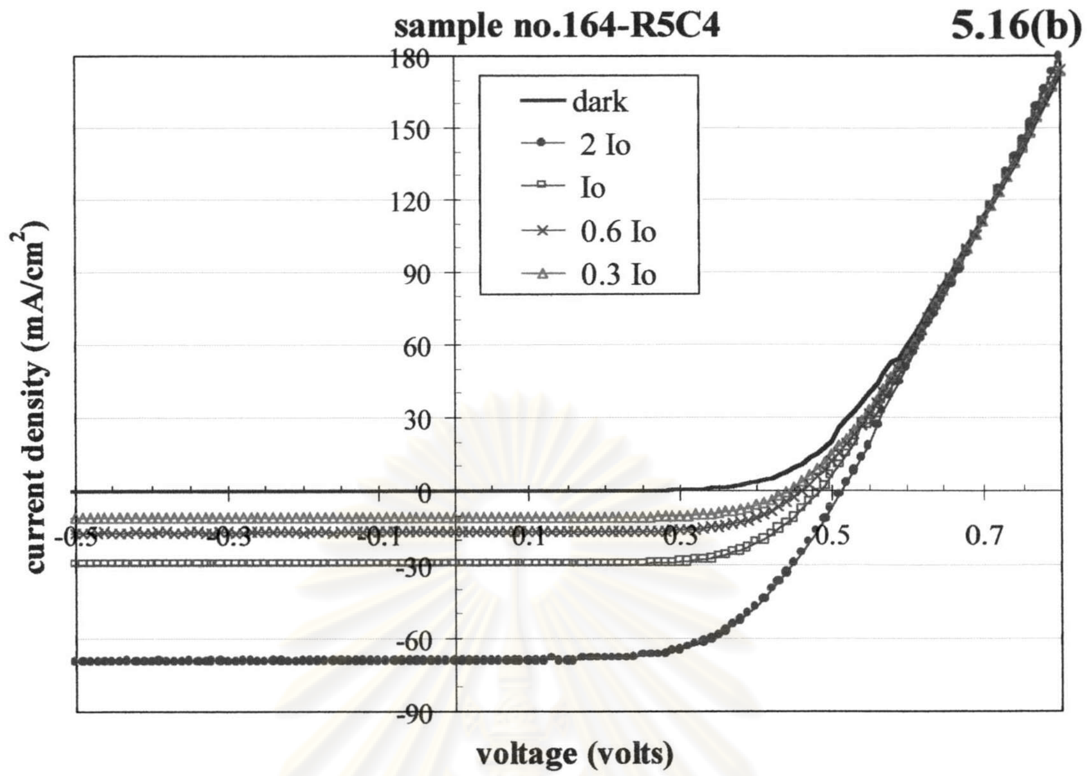

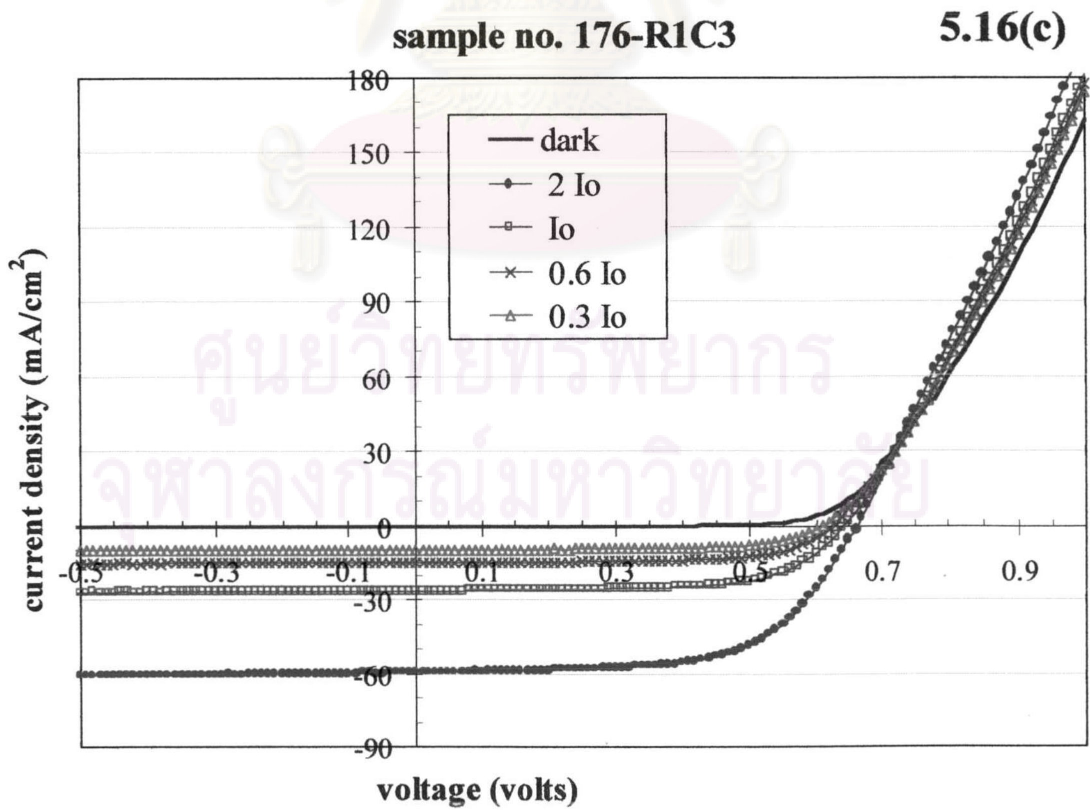

ศูนย์วิทยทรัพยากร
จุฬาลงกรณ์มหาวิทยาลัย

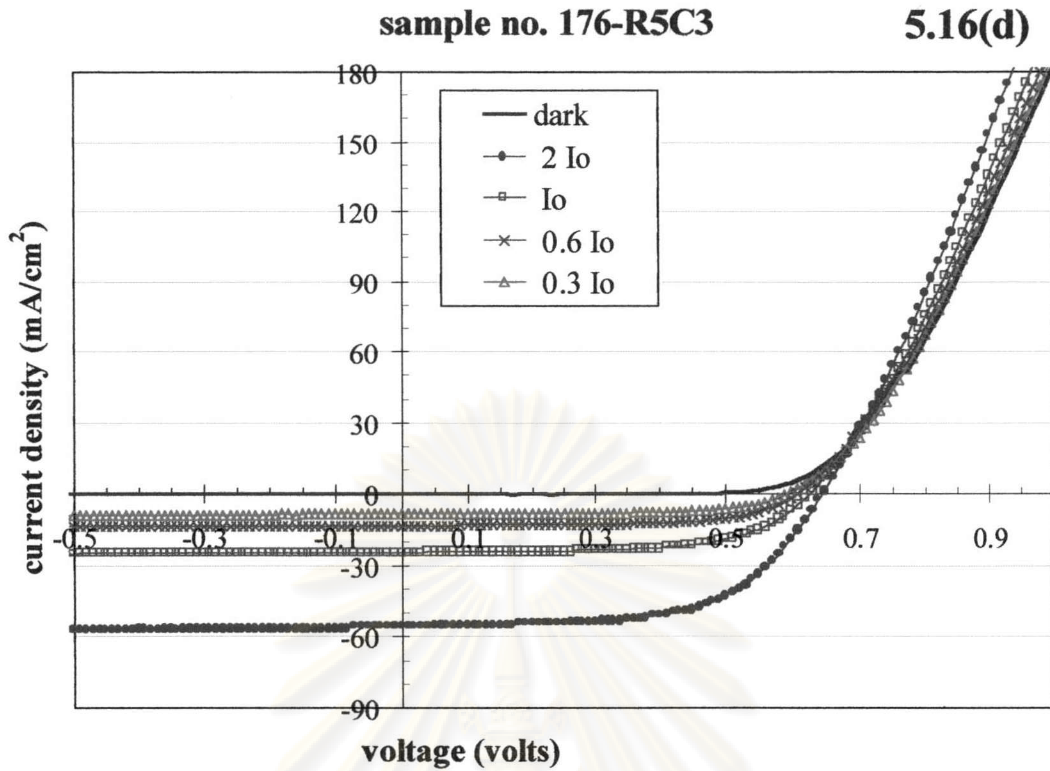

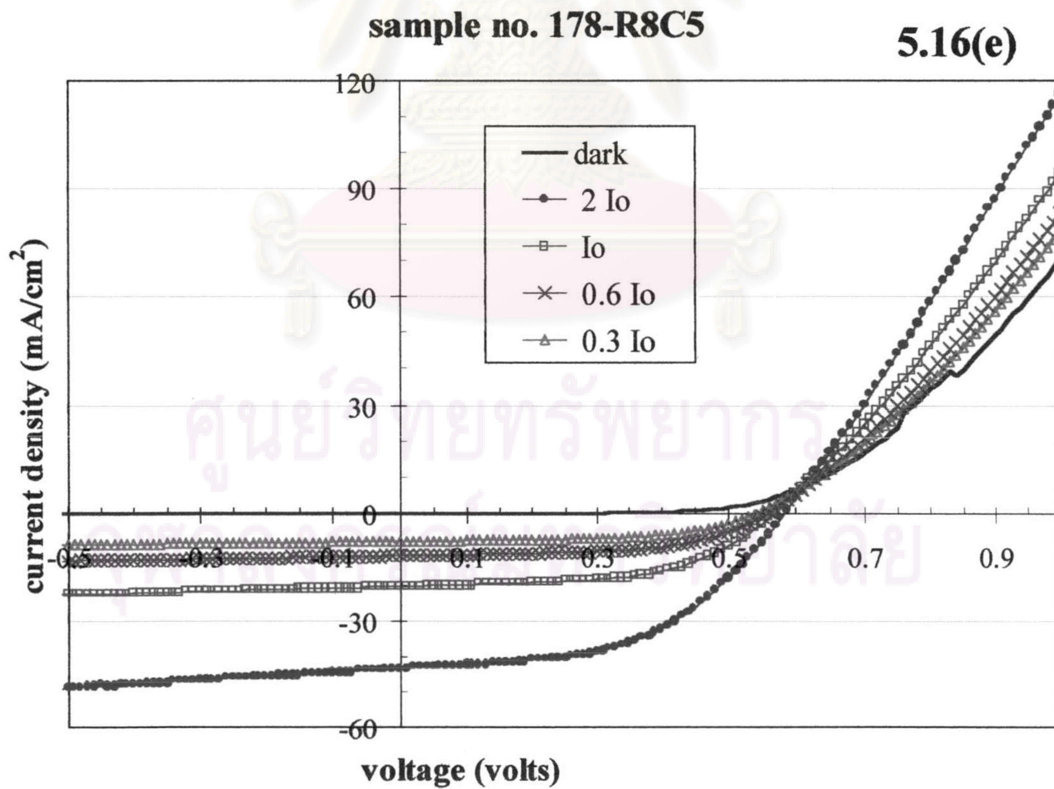

Figure 5.16: J-V characteristics of sample (a) no.164-R8C1, (b) no.164-R5C4, (c) no.176-R1C3, (d) no.176-R5C3, and (e) no.178-R8C5.

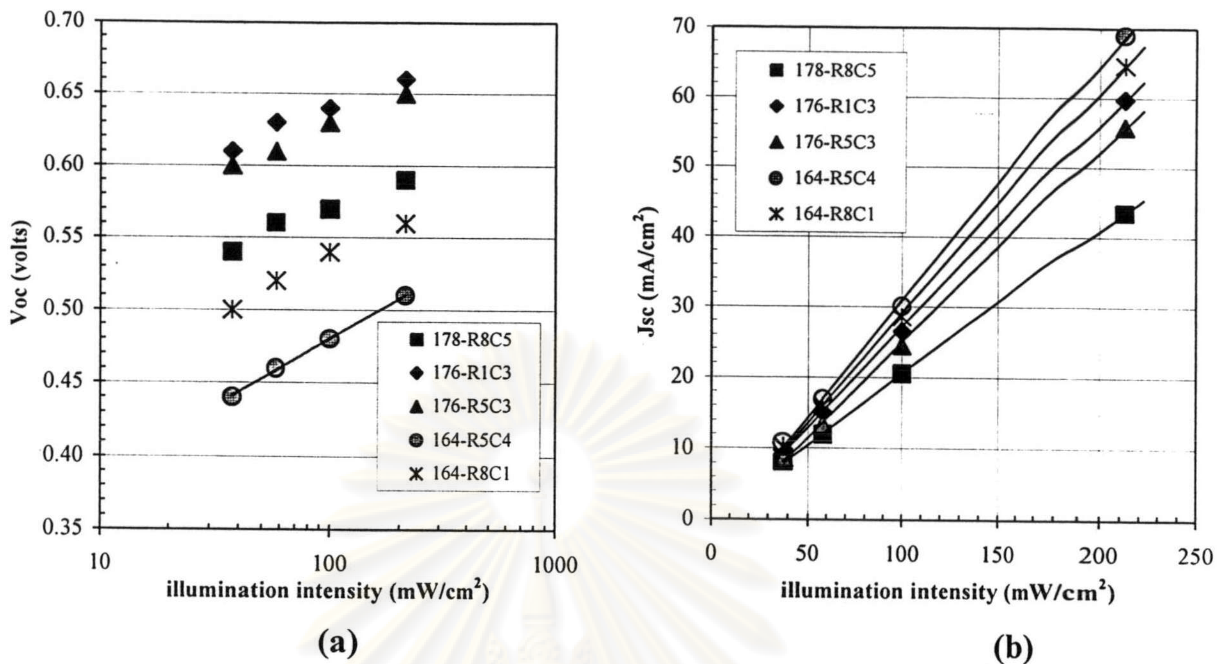

Figure 5.17: (a) V_{oc} vs. logarithm light intensity. (b) J_{sc} vs. light intensity plotted from five CIGS-based solar cell samples.

Figure 5.17(b) shows J_{sc} of each sample as a function of illumination intensity. From these results, J_{sc} of each sample is proportional to over all range of illumination intensity, from 30 to 220 mW/cm^2. Fig. 5.17(a) shows the linearly changed of V_{oc} with the logarithm of illumination intensity. As described in chapter 4, the J-V relation using diode model;

$$J \approx J_0 \exp\left(\frac{qV}{AkT}\right) - J_0 - J_L \ ,$$

and

$$V_{oc} \approx \left(\frac{AkT}{q}\right) \ln\left(\frac{J_{sc}}{J_0}\right) .$$

J_{sc} is proportional to illumination intensity (Fig. 5.17(b)) , so that we can estimate the diode ideality factor from the slope of V_{oc} vs. logarithm illumination intensity in Fig. 5.17(a). The result of approximation is $A \sim 1.55$ for sample no.164-R8C1. The obtained value corresponds with the value analyzed from the J-V

ศูนย์วิทยทรัพยากร
จุฬาลงกรณ์มหาวิทยาลัย

chracteristic under standard condition (see details in section 5.1). It can be concluded that the mechanism controlling the junction is SRH recombination in space charge region, in other words, no improvement on the recombination mechanism with increase the illumination intensity.

5.3.1 Light Soaking Effects

Many CIGS-based solar cell samples used in this research have distortion J-V characteristics such as crossover J-V and 2-diode-like J-V. These devices showed poor solar cell performances. The improvement of solar cell performances, using heat treatment or post annealing were reported [21]. In this experiment, I investigated the heat treatment or light soaking effect on the J-V characteristic of CIGS-based solar cell sample no 158-R1C5 whose J-V curves at standard condition (100 mW/cm^2 25°C) was 2-diode-like J-V curves. The light soaking effect on 2-diode-like J-V characteristic was shown in Fig. 5.18.

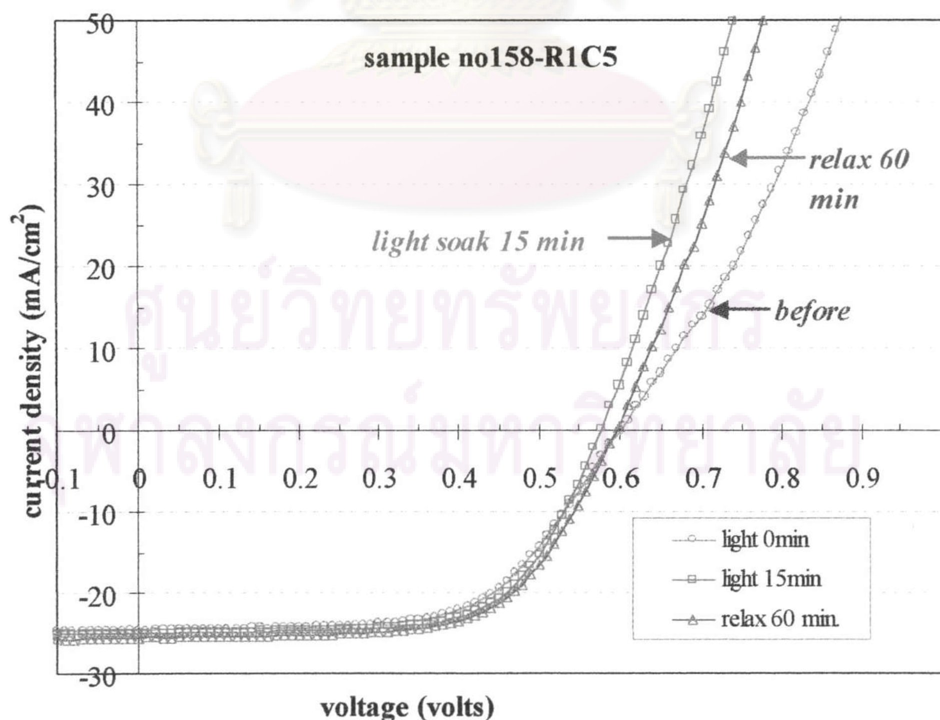

Figure 5.18: J-V characteristic of CIGS-based solar cell sample no.158-R1C5 during 15 minutes light exposure (at 25 °C under ELH light @ 100 mW/cm^2).

Figure. 5.18 shows the light soaking effect on the distortion J-V curves. The primary change in an improvement in the J-V curve is that the 2-diode-like J-V curves disappear, which, of course, increase the fill factor and efficiency. After relaxing in the dark for 60 minutes, the cell performance is essentially restored to its initial condition but the distortion J-V curve cannot be observed. The solar cell parameters of this sample no.158-R1C5 obtained before and after light soaking are shown in Fig. 5.19.

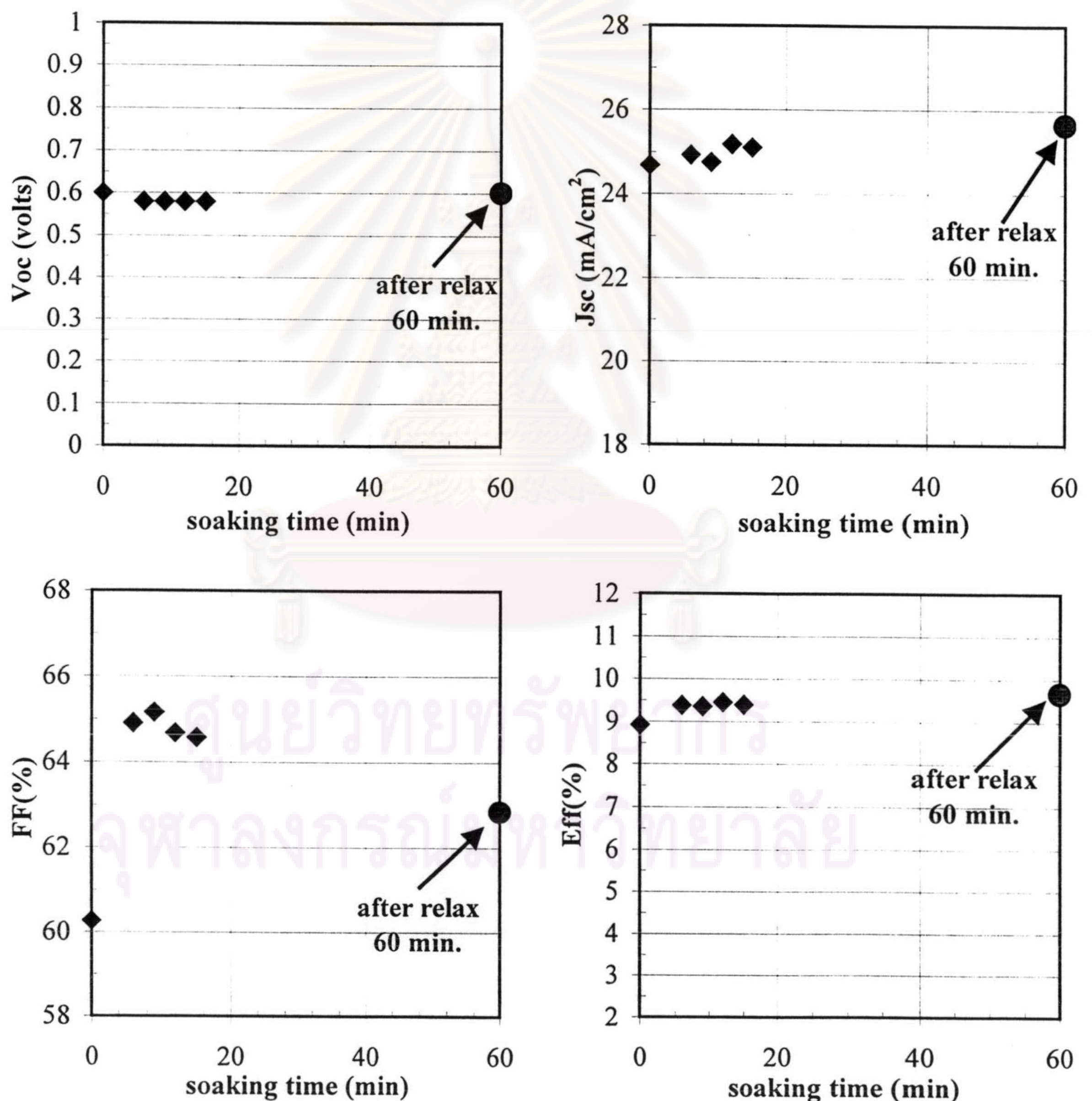

Figure 5.19: CIGS-based solar cell performances as a function of light exposure. Fill circles show the value after relaxing in the dark for 60 minutes.

Figure 5.19 shows the light exposure effect on the solar cell parameters. The most noticeable is an increase in fill factor and efficiency, but no observable change in V_{oc} after light soaking. The changes are rapid at first, but can continue at a reduced rate for long time. After relaxing in the dark (filled circles in Fig. 5.19), it is found that the improvement can also still compared with before light soaking. It could be described that the light exposure seems to almost eliminate the traps or the recombination centers at the interface resulting in the improvement of the junction formation, therefore, the device changes to the rectify diode.

5.4 Temperature Dependent Current-Voltage Characteristics [22-24]

Analysis of the current-voltage behavior of Cu(In,Ga)Se_2-based thin film solar cells has been used for understanding the mechanisms limiting V_{oc} and device performance. Previous results in section 5.1 have indicated that the primary mechanism controlling the junction behavior in samples ZnO/CdS/Cu(In,Ga)Se_2 thin film solar cells is Shockley-Read-Hall (SRH) recombination in the space charge region with the diode ideality factor A=1.5-2.0.

In this experiment, J-V characteristics were measured as a function of temperature. For temperature dependent current-voltage measurement, the sample was mounted inside a vacuum chamber with the possibility to cool down to 150 K and to heat up to 400 K. The temperature was measured by a thermocouple placed on the sample surface. The ELH type halogen lamp served as illumination normalized to 100 mW/cm^2. In the following, I show the temperature-dependence of current-voltage characteristics of ZnO/CdS/Cu(In,Ga)Se_2 heterojunction solar cells. For the evaluation of these experimental data, I took the current voltage

relation as described in section 3.2.2. The samples used in this experiment were prepared as described previously in chapter 4.

The J-V characteristic measurement as a function of temperature for two samples ZnO/CdS/Cu(In,Ga)Se_2 thin film solar cells are shown in Figs. 5.20 and 5.21.

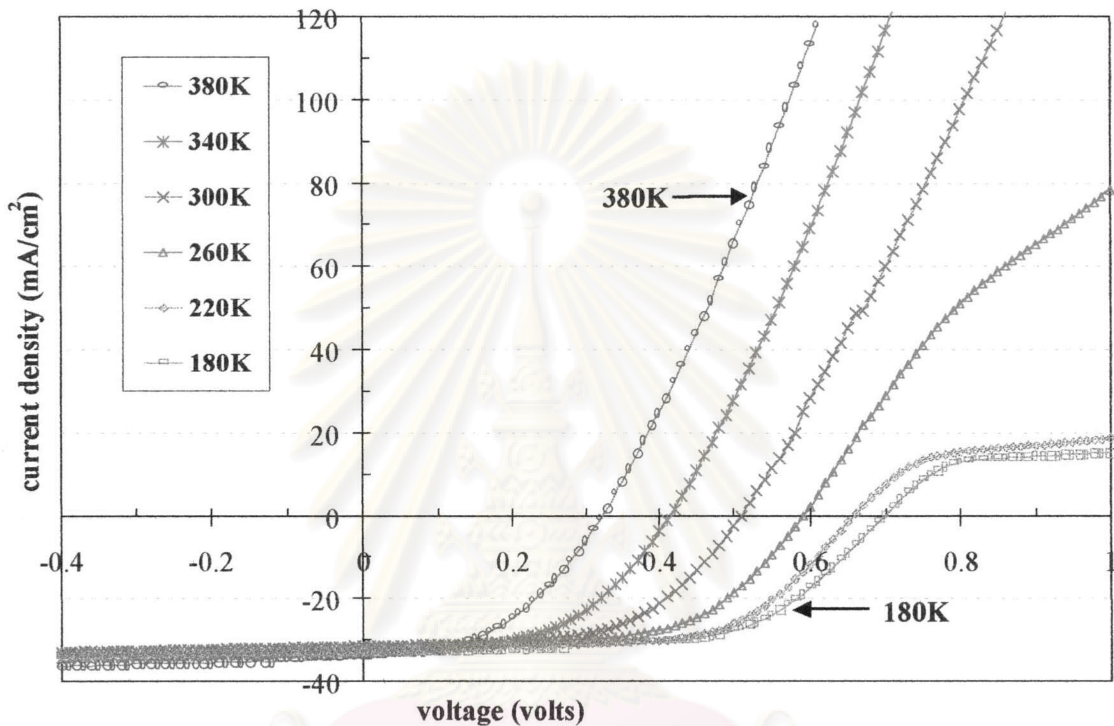

Figure 5.20: A plot showing current-voltage characteristics of ZnO/CdS/Cu(In,Ga) Se_2 solar cell sample no.123 as a function of temperature.

Figures 5.20 and 5.21 illustrate the J-V curves as a function of temperature of sample no.123 and no.68, respectively. All samples have non-linear contributions in series with the main diode, which are clearly observed in the forward bias J-V data at lower temperature. At low temperature (i.e. $T < 280\,\mathrm{K}$) the forward voltage bias behavior exhibits an increase in blocking behavior, which is a contribution due to a back diode. This has been reported [24] before and attributed to a non-ohmic Mo/Cu (In,Ga)Se_2 contact. This back diode does not affect V_{oc} but prevents analysis of

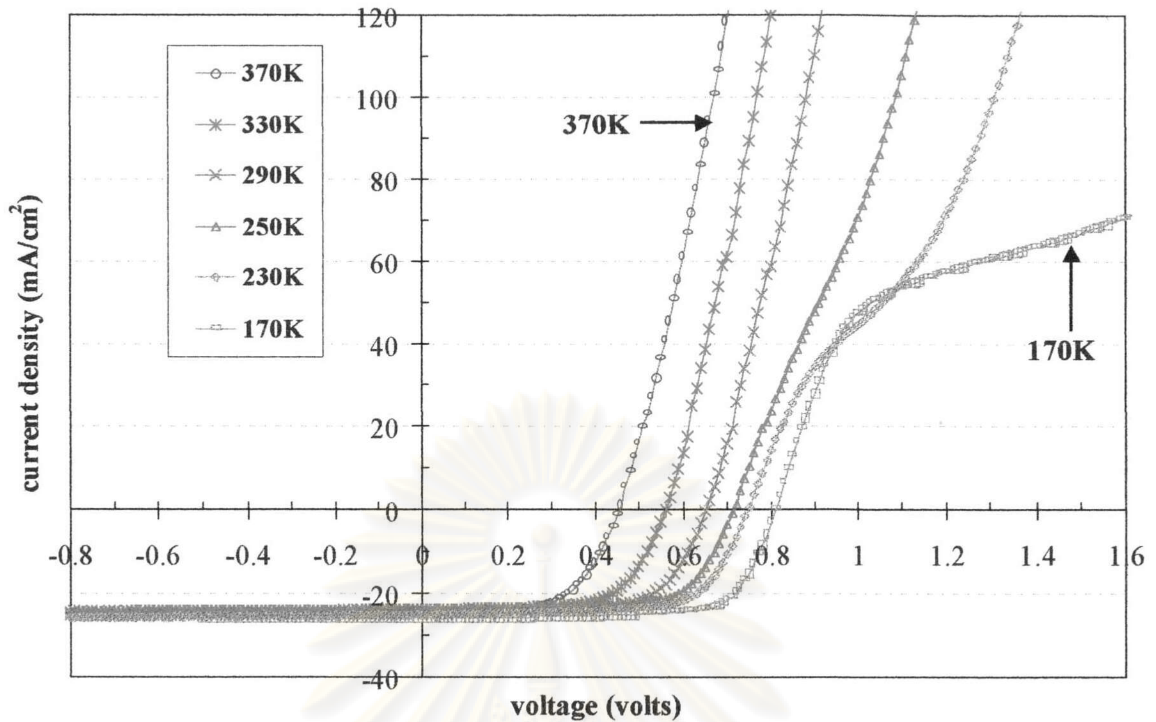

Figure 5.21: Current-voltage characteristics of ZnO/CdS/Cu(In,Ga)Se_2 solar cell sample no.68 as a function of temperature.

the J-V curves to determine the diode parameters. The full J-V characteristics can then be fitted using only a linear series resistance at higher temperature. Thus, the analysis is restricted to $T > 280\,\mathrm{K}$ for sample no.123.

The J-V relation for the CdS/Cu(In,Ga)Se_2 junction in presence of light can be described in term of a forward diode current and a light generated current in the opposite direction which includes linear series and shunt correction. The diode parameters A, R_s, and J_0 can be determined in the same method as described in section 5.1.

The J-V characteristics of the two samples used in this experiment under ELH illumination normalized to 100 mW/cm^2 AM1.5 at 25 °C are listed in Table 5.4.

Table 5.4: J-V parameters of CIGS-based solar cells studied in this experiment at 25 °C under AM1.5 illumination.

Sample no.	V_{oc} (volts)	J_{sc} (mA/cm^2)	FF (%)	η (%)
No.123	0.66	26.48	70.77	12.37
No.68	0.50	31.72	55.85	8.858

The following J-V relation was used to analyze the data with the results for sample no.123 given in Table 5.5.

Table 5.5: Diode parameters at different temperature for sample no.123.

Temp (K)	Voc (volts)	Jsc (mA/cm^2)	dark			illumination		
			A - factor	Jo (mA/cm^2)	Rs (Ω-cm^2)	A - factor	Jo (mA/cm^2)	Rs (Ω-cm^2)
370	0.45	25.72	1.516	2.0×10^{-4}	1.37	1.578	3.5×10^{-3}	1.34
360	0.47	25.92	1.546	1.0×10^{-4}	1.40	1.585	1.9×10^{-3}	1.39
350	0.5	25.59	1.622	1.0×10^{-4}	1.38	1.623	1.1×10^{-3}	1.41
340	0.53	26.19	1.677	7.0×10^{-5}	1.37	1.731	8.0×10^{-4}	1.37
330	0.56	25.31	1.703	4.0×10^{-5}	1.39	1.753	4.0×10^{-4}	1.43
320	0.59	25.68	1.732	2.0×10^{-5}	1.42	1.816	2.0×10^{-4}	1.42
310	0.62	25.22	1.746	1.0×10^{-5}	1.53	1.857	1.0×10^{-4}	1.47
300	0.64	26.11	1.757	8.0×10^{-6}	1.94	1.905	6.0×10^{-5}	1.57
290	0.65	25.94	1.88	9.0×10^{-6}	2.68	1.983	5.0×10^{-5}	1.91
280	0.66	24.77	2.086	5.0×10^{-6}	2.68	2.069	4.0×10^{-5}	2.08
270	0.67	25.06						
260	0.67	25.06						
250	0.67	25.76						
240	0.68	26.07						
230	0.7	25.86						
220	0.71	25.34						
210	0.72	25.38						
200	0.73	25.88						
190	0.74	26.02						
180	0.75	25.83						
170	0.75	25.74						

ศูนย์วิทยทรัพยากร
จุฬาลงกรณ์มหาวิทยาลัย

Table 5.5 shows diode parameters under dark and illumination, which J_0 and A are extracted from the J-V characteristics at higher bias after correcting the curve for R_s (see fitting procedure in section 5.1). I review the J-V relation used to analyze the J-V data [22].

$$J = J_0 \left\{ \exp \frac{q(V - R_s J)}{AkT} - 1 \right\} - J_{sc} + GV \tag{5.3}$$

with

$$J_0 = J_{00} \exp\left(-\frac{E_g}{AkT} \right) \tag{5.4}$$

At $J = 0$,

$$V_{oc} \approx \frac{AkT}{q} \ln\left(\frac{J_{sc}}{J_0} \right) \tag{5.5}$$

$$V_{oc} = \frac{E_g}{q} - \frac{AkT}{q} \ln\left(\frac{J_{00}}{J_{sc}} \right) \tag{5.6}$$

where E_g is the band gap energy of the absorber, and J_{00} is a prefactor which depends on the transport mechanism (tunneling or thermal activation) [11].

If A, J_{sc} and J_{00} in Eq.(5.6) are independent of temperature T, a plot of V_{oc} vs. T should yield a straight line and the extrapolation of this line to T=0 K gives the activation energy E_a. In case of interface recombination without tunneling, E_a leads to potential barrier.

In a similar way, one should be able to extract the band gap energy E_g of absorber layer by extrapolation of the V_{oc} vs. T plot if the diode ideality factor A depend on temperature T. In this case, when the tunneling becomes a major contribution to the recombination, the diode ideality factor becomes temperature dependent, inducing non-linear term into Eq. (5.6).

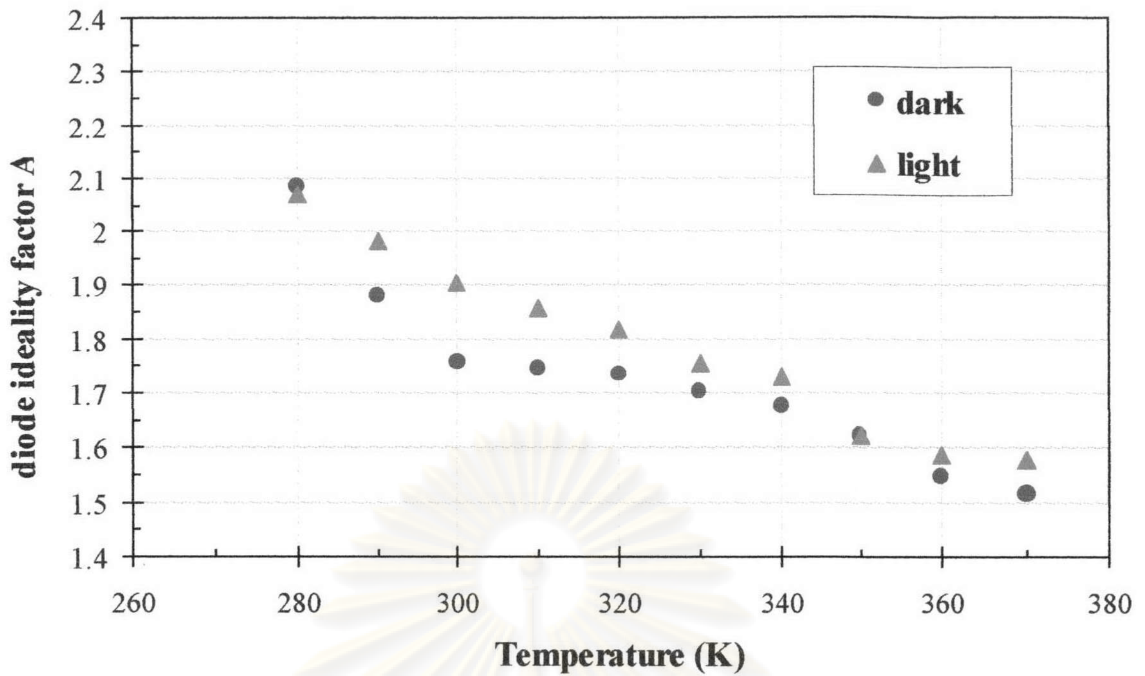

Figure 5.22: Diode ideality factor extracted from dark and light J-V characteristics.

Figure 5.22 shows that A strongly depends on temperature and the values of A are between 1 and 2 in a temperature range between 370 and 290 K. This indicates a thermally activated recombination via a distribution of trap states in the space charge region of the absorber material. For T < 290 K, A may increase above two due to an increased contribution of tunneling. The saturation current density J_0 in Eq.(5.4) can be rewritten as [14]

$$A\ln(J_0) = -\frac{E_g}{kT} + A\ln(J_{00}) \tag{5.7}$$

Thus, a plot of $A\ln(J_0)$ vs. the inverse temperature $1/T$ should yield straight line with a slope corresponding to the band gap energy E_g in case of bulk recombination, and correspond to the activation energy E_a in case of interface recombination. Figure 5.23 shows a plot of $A\ln(J_0)$ vs. the inverse temperature $1/T$ of sample no.123. The approximation of band gap energy of Cu(In,Ga)Se_2 absorber layer of sample no.123 obtained from slope is 1.14 eV.

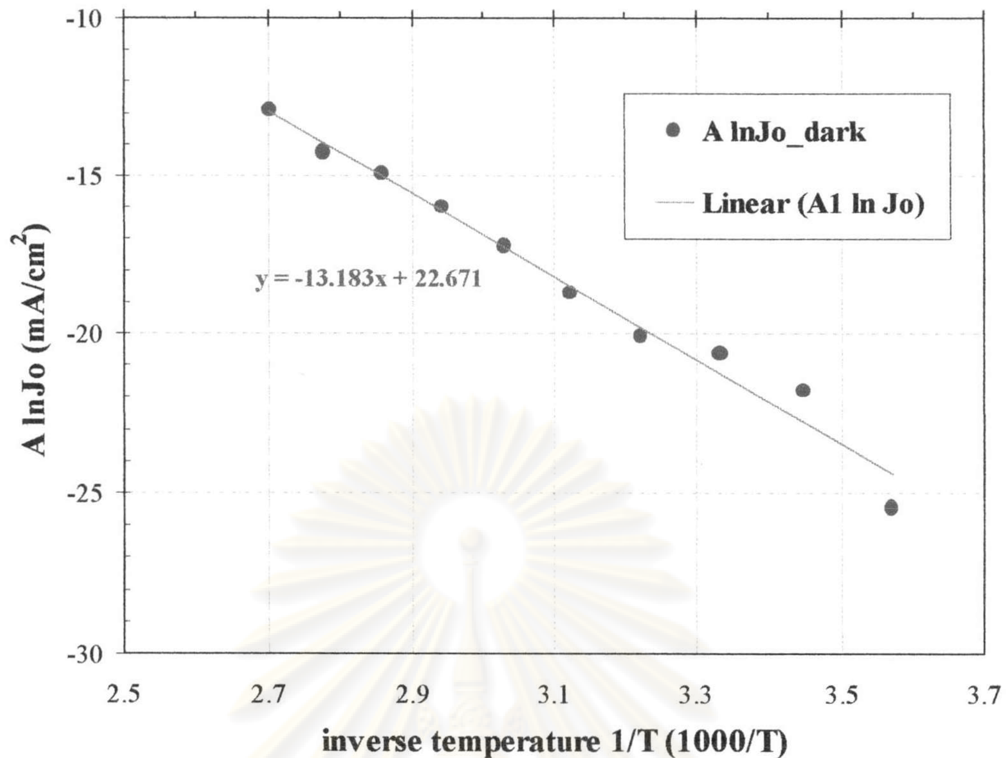

Figure 5.23: A plot of $A \ln J_0$ vs. the inverse temperature ($1/T$) of sample no.123. The slope yields the band gap energy of the absorber material of device ($E_g \approx 1.14\, eV$).

It can be concluded that the quantitative analysis of the temperature dependence of the diode ideality factor is required to decide in either case whether or not tunneling contributes significantly to recombination.

In addition, I examined the temperature dependence of the open circuit voltage V_{oc}. Assuming recombination via defect states, V_{oc} is determined by Eq. (5.6). The temperature dependence of V_{oc} is shown in Figs. 5.24 and 5.25 for sample no.123 and sample no.68, respectively.

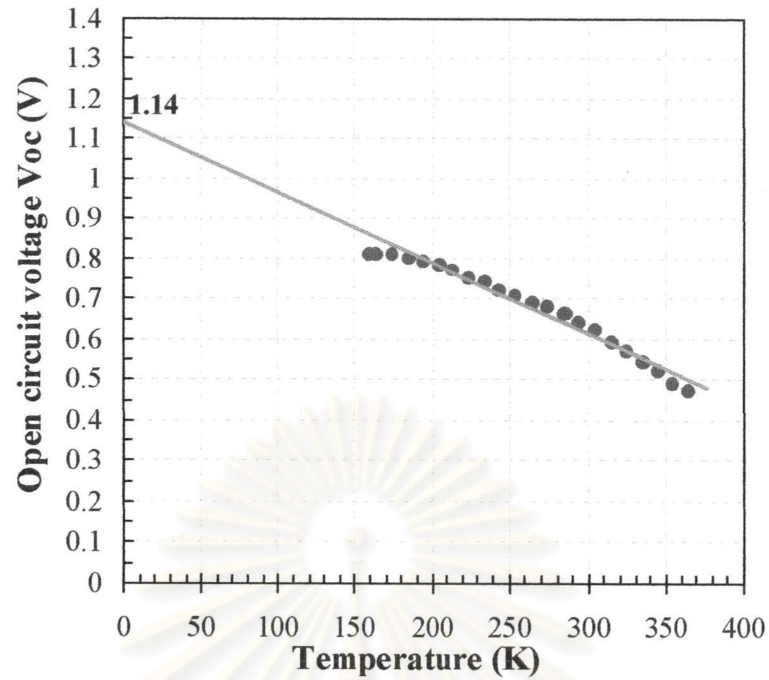

Figure 5.24: Temperature dependence of the open circuit voltage V_{oc} under illumination 100 mW/cm^2 of sample no.123.

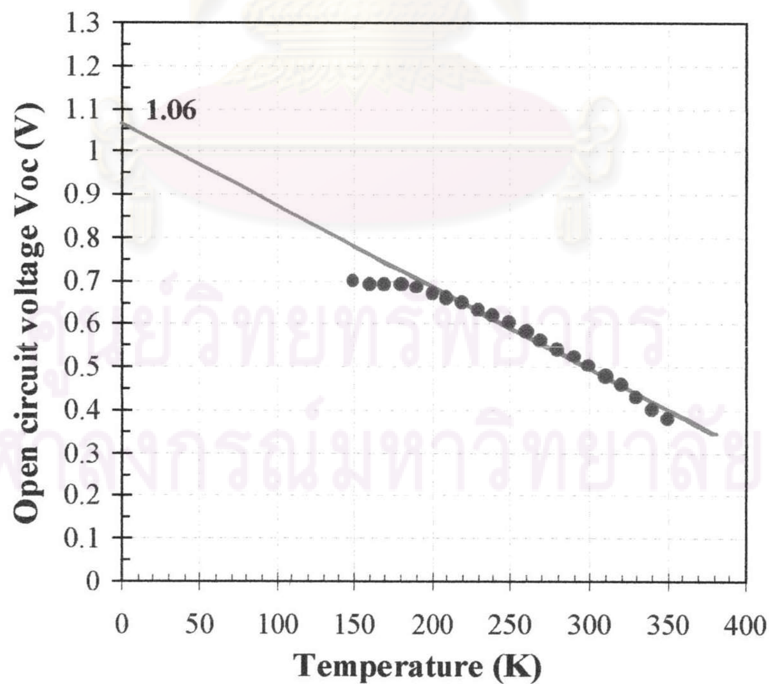

Figure 5.25: Temperature dependence of the open circuit voltage V_{oc} under illumination 100 mW/cm^2 of sample no.68.

Figures 5.24 and 5.25 show the temperature dependence of V_{oc}. For the extrapolation of V_{oc} vs. T, the open circuit voltages of samples no.123 and no.68 extrapolate to the values of approximately 1.14 V and 1.06 V, respectively, corresponding to the band gap energy of Cu(In,Ga)Se_2. These results show that if the recombinations occur via the trap states in the space charge region of the absorber dominating the extrapolation of V_{oc} vs. T correspond to E_g, whereas in case of interface recombination the extrapolation of V_{oc} vs. T corresponds to interface barrier height.

From the above results, the analysis of the J-V characteristics of Cu(In,Ga)Se_2-based thin film solar cells begin with a diode equation which includes linear series and shunt corrections. However, it cannot generally be assumed that these linear corrections are sufficient to represent the measured J-V data dependence of temperature. The illumination J-V curves have non-linear characteristics in forward bias which are visible at lower temperature. The junction behavior is determined at V_{oc}, where series effects in the device do not contribute, and found to have the same basic diode behavior.

From the low temperature J-V characteristic under illumination presents the back diode in series with the main heterojunction solar cell [24]. The back diode most probably a schottky type at the Mo/Cu(In,Ga)Se_2 junction. However, the back diode or non-ohmic contact behavior does not have any effect on the open circuit voltage and is therefore assumed to occur in series with the primary diode. This behavior may originate at Mo/Cu(In,Ga)Se_2 or changes in the electrical properties of the Cu(In,Ga)Se_2/CdS junction. Thus, the high efficiency Cu(In,Ga)Se_2-based thin film solar cell is modeled by the equivalent circuit illustrated in Fig. 5.26.

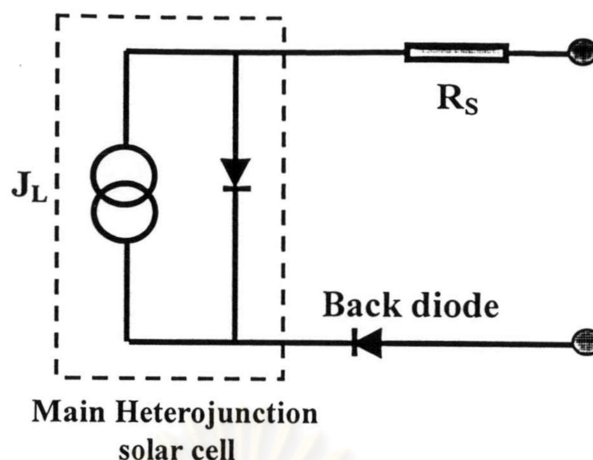

Figure 5.26: Equivalent circuit of $Cu(In,Ga)Se_2/CdS$ heterojunction solar cell including the back diode in series with the main heterojunction.

5.5 Proposed Band Model

The construction of the energy band diagram of $ZnO/CdS/Cu(In,Ga)Se_2$ heterojucntion proceeds by first drawing the energy diagrams for the materials separately as in Fig. 5.27(a) with the vacuum level of energy common. The parameters used for the proposed of energy band diagram are shown in Table 5.6.

ศูนย์วิทยทรัพยากร
จุฬาลงกรณ์มหาวิทยาลัย

Table: 5.6 Parameters used for the propose of energy band diagram of $Cu(In,Ga)Se_2$-based thin film solar cell [18].

Material	Band gap energy E_g (eV)	Work function ϕ (eV)	Electron affinity χ (eV)
Mo	-	4.3	-
CIGS	1.11	-	-
CdS	2.42	7.26	4.1
ZnO	3.3	-	4.3

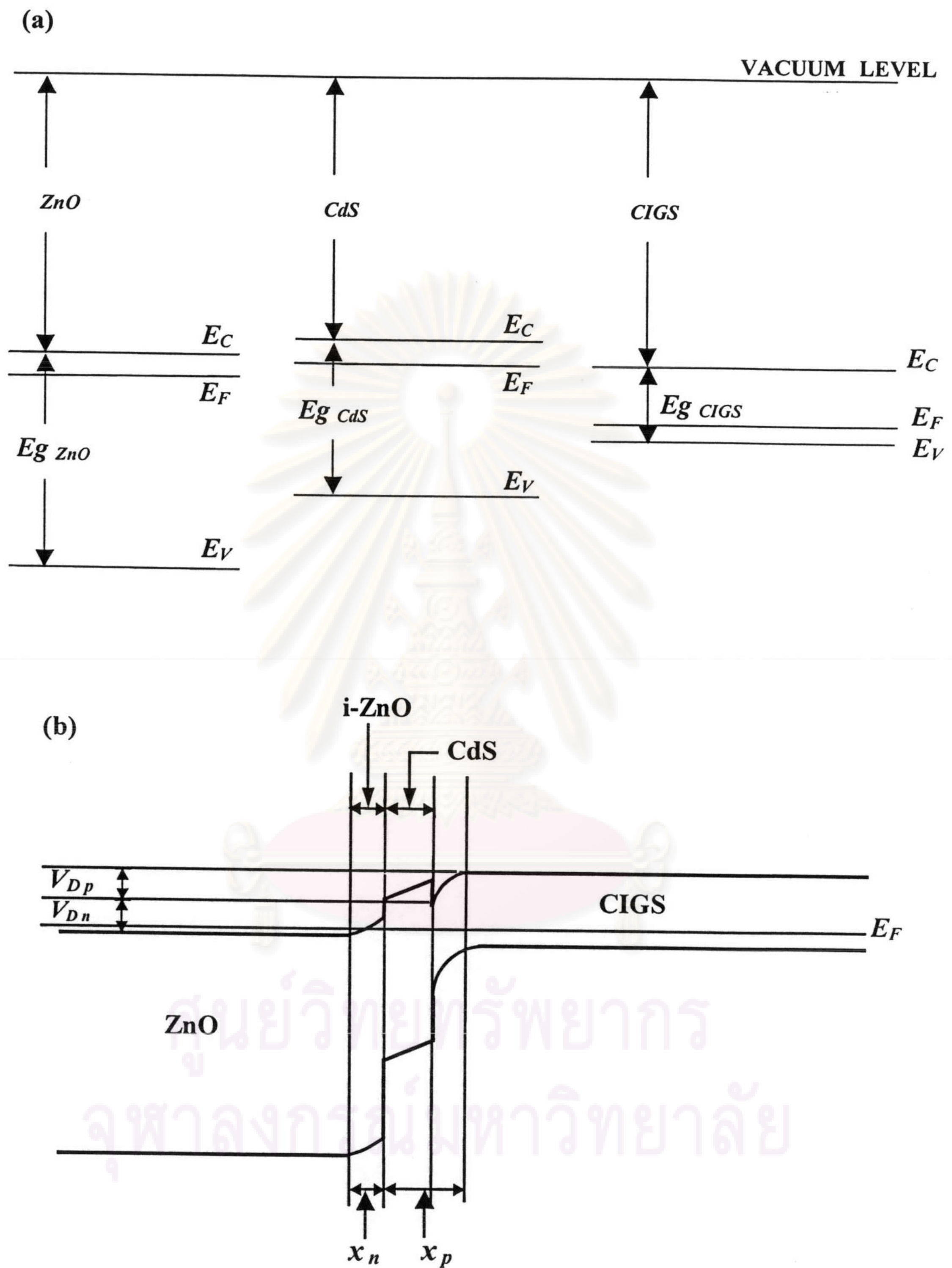

Figure: 5.27 Schematic of energy band diagram before (a), and after (b) the formation of ZnO/CdS/Cu(In,Ga)Se_2 heterojunction.

From Fig. 5.27, the Fermi level of p-CIGS E_{Fp} is lower in electron energy than that of n-CdS E_{Fn}. Define the band bending in n-side and p-side are V_{Dn} and V_{Dp}, respectively. The Fermi level displacement $E_{Fp} - E_{Fn}$ can be written as

$$E_{Fp} - E_{Fn} = (\chi_{CIGS} + E_{gCIGS} - \delta_{CIGS}) - (\chi_{CdS} + \delta_{CdS})$$

$$= V_{Dn} - V_{Dp} \ , \tag{5.8}$$

with

$$\delta_{CIGS} = (E_F - E_V)_{CIGS} \ , \tag{5.9}$$

and

$$\delta_{CdS} = (E_C - E_F)_{CdS} \ . \tag{5.10}$$

The total built-in voltage V_D due to the difference in work functions is equal to the sum of built-in voltage on both sides

$$V_D = V_{Dn} + V_{Dp} \ . \tag{5.11}$$

The depletion width in p-type x_p and in n-type x_n can be written as

$$x_p = \left(\frac{2}{q} \frac{N_A \varepsilon_p \varepsilon_n V_D}{N_D (\varepsilon_p N_A + \varepsilon_n N_D)} \right)^{1/2} , \tag{5.12}$$

$$x_n = \left(\frac{2}{q} \frac{N_D \varepsilon_p \varepsilon_n V_D}{N_A (\varepsilon_p N_A + \varepsilon_n N_D)} \right)^{1/2} , \tag{5.13}$$

where ε_p and ε_n are dielectric constant in p-type and n-type respectively, N_A and N_D are concentration of acceptor in p-type and donor in n-type respectively.

The relation between V_{Dn} and V_{Dp} is

$$\frac{V_{Dp}}{V_{Dn}} = \frac{N_D \varepsilon_n}{N_A \varepsilon_p} \ . \tag{5.14}$$

When an external voltage V is applied across such a junction, then the Eqs. (5.8)-(5.14) can be written by replacing V_D by $(V_D - V)$, replace V_{Dp} by $(V_{Dp} - V_p)$ and replace V_{Dn} by $(V_{Dn} - V_n)$, as $V = V_p + V_n$, hence

$$\frac{V_{Dp} - V_p}{V_{Dn} - V_n} = \frac{N_D \varepsilon_n}{N_A \varepsilon_p} \ . \tag{5.15}$$

With this proposed band diagram of $ZnO/CdS/Cu(In,Ga)Se_2$, the J-V characteristics in this research can be described as following:

The J-V characteristics from the standard measurement in this research can be divided into three groups of features, the first is normal J-V, the second is the crossover J-V and the third feature is the 2-diode like J-V curve.

1. Normal J-V characteristics

   In this case, the CdS/CIGS interface has low concentration of interface states or traps. These traps do not affect on the depletion width of both sides under dark and illumination. With apply forward bias voltage under dark and illumination, rate of decreasing in the depletion width of both sides is equal. Thus the superposition principle between dark and illuminated J-V is valid.

2. Crossover J-V characteristics

   In this case, the concentration of the traps at CdS/CIGS interface is high enough. When the junction is under illumination, the traps will be occupied by the photogenerated electron-hole pairs resulting in the density of donor N_D different from N_D under dark situation. Consequently, the rate in decreasing of depletion width of both sides and flat band voltage under illumination is smaller than under dark situation. Thus, the crossover I-V curves appear.

3. 2-diode like J-V characteristics

   In this case, the 2-diode like I-V curves correspond to the difference in the rate of decreasing in depletion width of both sides resulting from the high density of trap states in CdS layer and ZnO/CdS interface. It results in splitting of the built-in voltage into two potential with different gradients, i.e., one across the n-ZnO and the othere across the CdS/CIGS interface [25]. Under illumination situation with forward bias, voltage across ZnO is unaffected while voltage across CdS/CIGS flattens. With apply more bias,

the electron concentration cannot increase exponentially with the bias due to the potential barrier. When pass the V_{oc}, more electron exist in the CdS, lowering the voltage across ZnO/CdS interface. Therefore, the current resumed exponential increase.

5.6 Conclusions

In this chapter, I demonstrated the current-voltage characteristics, and used the 1-diode model to determine the mechanism controlling the junction behavior. The results show the dominant mechanism controlling the junction current of $Cu(In,Ga)Se_2$-based thin film solar cells at room temperature is SRH-recombination in space charge region. I also discussed the J-V characteristics measured as a function of temperature, which the results show that at low temperature diode ideality factor increase above two due to an increased contribution of tunneling. I also described the impurities in the CBD-CdS layer and the illumination intensity effect on the J-V characteristics, including I proposed the possible energy band diagram of $ZnO/CdS/Cu(In,Ga)Se_2$ heterojunction.

ศูนย์วิทยทรัพยากร
จุฬาลงกรณ์มหาวิทยาลัย